The Astrophysical Journal, 715:1539–1555, 2010 June 1 doi:10.1088/0004-637X/715/2/1539

SEISMIC AND DYNAMICAL SOLAR MODELS. I. THE IMPACT OF THE SOLAR ROTATION HISTORY ON NEUTRINOS AND SEISMIC INDICATORS

S. Turck-Chièze[1], A. Palacios[1,2], J. P. Marques[3], and P. A. P. Nghiem[1,4]
[1] CEA/DSM/IRFU/Service d'Astrophysique, CE Saclay, L'Orme des Merisiers-bât 709, F-91191 Gif-sur-Yvette, France; Sylvaine.Turck-Chièze@cea.fr
[2] GRAAL, Université Montpellier II, CNRS, place Eugène Bataillon, F-34095 Montpellier, France; Ana.Palacios@univ-montp2.fr
[3] Observatoire de Paris, 92 Meudon, France; Joao.Marques@obspm.fr
Received 2009 December 13; accepted 2010 April 3; published 2010 May 12

ABSTRACT

Solar activity and helioseismology show the limitation of the standard solar model and call for the inclusion of dynamical processes in both convective and radiative zones. In this paper, we concentrate on the radiative zone. We first recall the sensitivity of boron neutrinos to the microscopic physics included in solar standard and seismic models. We confront the neutrino predictions of the seismic model with all the detected neutrino fluxes. Then, we compute new models of the Sun including a detailed transport of angular momentum and chemicals due to internal rotation that includes meridional circulation and shear-induced turbulence. We use two stellar evolution codes: CESAM and STAREVOL to estimate the different terms. We follow three temporal evolutions of the internal rotation which differ by their initial conditions: very slow, moderate, and fast rotation, with magnetic braking at the arrival on the main sequence for the last two. We find that the meridional velocities in the present solar radiative zone are extremely small in comparison with those of the convective zone (smaller than 10^{-6} cm s^{-1} instead of m s^{-1}). All models lead to a radial differential rotation profile in the radiative zone but with a significantly different contrast. We compare these profiles to the presumed solar internal rotation and show that if meridional circulation and shear turbulence were the only mechanisms transporting angular momentum within the Sun, a rather slow rotation in the young Sun is favored. We confirm the small influence of the transport by rotation on the sound speed profile but its potential impact on the chemicals in the transition region between radiation and convective zones. These models are physically more representative of the real Sun than the standard or seismic solar models but a high initial rotation, as has been considered previously, increases the disagreement with neutrinos and the sound speed in the radiative zone. This present work pushes us to pursue the inclusion of the other dynamical processes to better reproduce the observed solar profile in the whole radiative zone and to better describe the young active Sun. We also need to get a better knowledge of solar gravity mode splittings to use their constraints.

Key words: hydrodynamics – neutrinos – Sun: evolution – Sun: helioseismology – Sun: interior – Sun: rotation

Online-only material: color figures

1. INTRODUCTION

Evidence for the presence of dynamical processes exists in stars all over the Hertzsprung–Russell (H-R) diagram. In the case of the Sun, rotation and magnetic activity have been confirmed for more than four centuries. Rapid rotation is found mainly in young stars and intermediate-mass to massive stars while mild to slow rotation is found in low-mass stars and in giant stars. Kraft (1965) was the first to study in detail the projected rotational velocity $v\sin i$ of young stars in clusters and show the transition between rapid rotation for early-type stars and slow rotation for late-type stars. Then, Weber & Davis (1967) explained that the angular momentum loss is due to a magnetized wind in solar-like stars. In studying Pleaides, Ursa Major, and Hyades, Skumanich (1972) used solar and cluster data to establish the law of variation of the rotation with age; this simple law is in fact more complex and has been studied in great detail for different masses (Stauffer et al. 1987; Bouvier 1994; Maeder & Meynet 2000, 2004; Bouvier 2009).

Rotation affects the internal stellar structure and evolution both directly via the modification of the gravitational potential, and by means of associated transport processes. It has a direct impact on the shape of stars, that can be directly probed with interferometric data for the strongly deformed fast rotating stars (Domiciano de Souza et al. 2003; McAlister et al. 2005; van Belle et al. 2006; Kervella & Domiciano de Sousa 2006; Domiciano de Souza 2008). In the case of the Sun, the effect is small as shown in Piau & Turck-Chièze (2002) but of considerable importance (Zahn 2009; Rozebt 2009) to check the influence of the deep core rotation and of the deep magnetic field (Duez et al. 2010a, 2010b) on the tachocline and on the solar surface.

The standard solar and stellar evolution models do not take into account the effects of such dynamical processes as rotation or magnetic fields. If helioseismology required the improvement of the solar model and motivated the introduction of microscopic diffusion, going beyond the zero-order model, it is the far too rough agreement between observational data and theoretical predictions for other stars that has led to the progressive introduction of the dynamical physical processes likely to affect the transport of momentum and chemicals in the stellar evolution codes. Using either a purely diffusive approach (Endal & Sofia 1981; Pinsonneault et al. 1989; Chaboyer et al. 1995; Langer 1998; Heger et al. 2000) or the more complex formalism developed by Zahn (1992) and Maeder & Zahn (1998), the introduction of the rotation-induced transport of angular momentum and chemicals to model both massive and low-mass stars improves the comparison with observations (see, e.g., Meynet & Maeder 2000; Talon & Charbonnel 1998;

[4] P. A. P Nghiem has now left the Service d'Astrophysique in IRFU/CEA and works in another discipline in the same institute.

Palacios et al. 2003). These results encourage us to pursue this effort for the Sun to get a proper interpretation of the existing helioseismic observations and the coming asteroseismic ones.

Acoustic and gravity mode detections provide a unique insight on the internal solar sound speed, density, and rotation profiles (Kosovichev et al. 1997; Turck-Chièze et al. 2001b; Thompson et al. 2003; Couvidat et al. 2003b; Turck-Chièze et al. 2004a; Mathur et al. 2007, 2008). This gives us a unique opportunity to validate the complex formalism introduced in rotating stellar evolution models. This information justifies the development of a dynamical solar model (DSM) to be confronted with the helioseismic and neutrino probes. The solar status must improve our knowledge of solar-like stars where only external stellar rotation rates or abundance anomalies are used to confront theoretical assumptions to observational facts. Moreover, building a consistent dynamical evolution model for the Sun will largely contribute to establish a complete and consistent MHD representation of the Sun and a good connection between internal and external magnetism.

The inner solar rotation is the first evidence of the internal dynamics that needs to be understood. This is not an easy task because the present-day profile results from the interplay between several distinct processes (Zahn et al. 1997; Chaboyer et al. 1995; Eggenberger et al. 2005; Charbonnel & Talon 2005) and their influence depends on the adopted theoretical prescriptions. The most recent of these studies include the transport of angular momentum by magnetic field or internal gravity waves, in addition to the "purely" rotational transport by meridional circulation and shear-induced turbulence, to obtain a more efficient extraction of angular momentum and a relative flat rotation profile in the radiative interior in better agreement with helioseismic data. Actually, both magnetic field and internal gravity waves probably contribute to the transport of angular momentum in stellar interiors, yet no models have been published up to now including all the processes. Moreover, the way to account for the effect of magnetic fields in one-dimensional stellar evolution codes is still puzzling and a matter of debate, and the introduction of gravity waves produces some irregularities in the radiative rotation profile (see, e.g., Charbonnel & Talon 2005) in disagreement with the helioseismic results.

In the present paper, we limit ourselves to the sole effect of rotational transport and carefully study the hypotheses and the order of magnitude of the terms that we introduce for the inner rotation. This approach pushes further the previous works by Chaboyer & Zahn (1992), Chaboyer et al. (1995), Charbonnel & Talon (2005), Eggenberger et al. (2005), Yang & Bi (2006), and Yang & Bi (2007). We focus our analysis on the solar core and we compare our results with all the recent existing seismic and neutrino indicators. This paper is a first of a series where we will discuss in details the influence of rotation, magnetic field, and internal waves on the solar dynamical model. We do not present and discuss the abundances of lithium and beryllium as it has been done extensively by Pinsonneault et al. (1989). Indeed, we have shown in our previous works on the tachocline (Brun et al. 1999) and on young stars that the abundance of these elements is sensitive to the early evolution as well as to the presence of the tachocline. These studies lead us to the conclusion that we need to treat properly the magnetic field in the early phase to better estimate the lithium evolution during this phase (Piau & Turck-Chièze 2002).

In Section 2, we present the status of the solar classical models and compare the seismic model predictions to all the present detected neutrinos. Then in Section 3, we recall the formalism proposed by Zahn (1992) and Maeder & Zahn (1998), and slightly improved by Mathis & Zahn (2004) that we use to introduce the rotation effects in the stellar evolution codes. In that section, we also give a brief description of the CESAM and STAREVOL stellar evolution codes used in the paper, and present the three different types of solar models which differ by their initial rotation and the presence of magnetic braking. In Section 4, we compare the results of these three rotating solar models obtained with both codes. These models are compared with seismic observations and neutrino detections in Section 5. In the last section, we summarize the important points in a more general context.

2. THE MICROSCOPIC PROCESSES AND THE SOLAR PROBES

The Sun differs from other stars by its proximity and our ability of observation. We know its luminosity, radius, and mass better than any other star. This has, for a long time, turned the Sun into a reference for stellar evolution. Nevertheless, the numerous constraints point to flagrant limitations of the standard picture:

1. In this framework, the luminosity increases by 30% in 4.6 Gyr, 8% during the last Gyr, and by only 10^{-8} during the last century. But in fact, the so-called solar constant shows variations by about 10^{-3} in mean value (Fröhlich 2006) correlated to the solar cycles (active cavity radiometer irradiance monitor (ACRIM) and *Solar and Heliospheric Observatory* (*SoHO*) observations). The presence of faculae around the sunspots explains the increase of luminosity at the maximum of the cycle. Moreover, the series of data shows clearly short timescale luminosity variation connected to the rotation and the presence or absence of sunspots in the field of view. This fact shows, just from fundamental quantities, that the standard framework is not sufficient and that magnetism and rotation must be introduced in the solar structural equations to interpret these observations because it is believed that these manifestations have an internal origin (Turck-Chièze & Lambert 2007; Duez et al. 2010a).
2. We have learned recently that the absolute irradiance is not so well established. The SORCE satellite suggests a reduction of nearly 6 W m^{-2} (Kopp et al. 2005) in comparison with the standard (3.846 ± 0.00410^{33} erg s^{-1} corresponding to 1367.6 W m^{-2}) used for solar models (see Bahcall & Pinsonneault 1995). This result modifies by 1.5–2 W m^{-2} (340 instead 342 W m^{-2}) the energy which reaches the stratosphere. So, the present solar luminosity value, which is used to calibrate the standard model, is presently uncertain at 0.5% (Turck-Chièze & Lefebvre 2010). The calibration and ageing of the radiometers are difficult to estimate, so the use of the space data is not easy. The SORCE/TIM instrument has an estimated absolute accuracy of 350 ppm and a long-term repeatability of 10 ppm per year. Nevertheless, the analysis of the 30 years data series seems to show a slow decrease of the total luminosity (Fröhlich 2006) between successive minima which cannot be understood in the standard solar framework.
3. For three decades, our star has also been scrutinized by two probes of the interior (neutrinos and seismic modes) that help us to largely progress in our capability to check

Table 1
Time Evolution of the Boron Neutrino Flux Prediction (Expressed in 10^6 cm^{-2} s^{-1}) Associated with the Reaction ^{7}Be$(p,\gamma)^8$B $\longrightarrow$ ^{8}Be $*$ $+e^+ + \nu_e \longrightarrow$ ^{4}He, for Calibrated Solar Structural Models

Year	Boron Neutrino Flux	T_c	Y_0	Problem Solved
Turck-Chièze et al. (1988)	3.8 ± 1.1	15.6	0.276	SSM CNO opacity, ^{7}Be(p,γ)
Turck-Chièze & Lopes (1993)	4.4 ± 1.1	15.43	0.271	SSM Fe opacity, screening
Brun et al. (1998)	4.82	15.67	0.273	SSM microscopic diffusion
Brun et al. (1999)	4.82	15.68	0.272	SSM turbulence in tachocline
Turck-Chièze et al. (2001b)	4.98 ± 0.73	15.74	0.276	SSeM
Couvidat et al. (2003a)	5.07 ± 0.76	15.75	0.277	SSeM +magnetic field
Turck-Chièze et al. (2004a)	3.91 ± 1.1	15.54	0.262	SSM Asplund et al. (2004) composition
Turck-Chièze et al. (2004a)	3.98 ± 1.1	15.54	0.262	SSM Holweger (2001) composition
Turck-Chièze et al. (2004a)	5.31 ± 0.6	15.75	0.277	SSeM and new ^{7}Be(p, γ), ^{14}N(p,γ)
Present work	5.31 ± 0.6	15.75	0.277	SSeM
	4.21	15.51	0.262	SSM Asplund et al. (2009) composition
	5.09	15.64	0.273	SSM GN and DSM1 GN with slow rotation
	4.52	15.54	0.269	DSM1 GN moderate rotation

Notes. Also mentioned are the corresponding central temperature T_c, initial helium content Y_0, and the origin of the improvements introduced in the corresponding solar model.

the internal solar plasma in great detail. We are now able to disentangle the production of neutrinos for specific nuclear reactions like ^{7}Be(p, γ) and ^{8}B(p, γ), and to sum the different flavors to really estimate the number of emitted neutrinos. The quality of the detection of the boron neutrinos (see Section 2.2 and Table 1), is such that the central temperature of the Sun is now known to about 0.5%. Neutrinos can thus bring very strong constraints to the solar models. On the helioseismic side, the detection of million acoustic modes stimulated a real insight on the thermodynamics of the radiative region (see below) and on the dynamics of the convective zone. Gravity modes also appear promising to reveal the last missing information, the dynamics of the solar core (Turck-Chièze et al. 2004b; García et al. 2007, 2008; Mathur et al. 2007, 2008).

2.1. The Validity of the Standard Solar Model

The solar radiative zone represents 98% of the total mass of the Sun and the adopted microphysics plays a basic role in this region. The equilibrium between gravitational energy, nuclear energy production, and the energy escaping by photon interaction needs to be followed in the radiative interior over long timescales. This region is now permanently probed by helioseismology, which is a key to validate the various ingredients used in the construction of the standard solar model (SSM). One success of the *SoHO* space observatory has been obtained by measuring the Doppler velocity shifts down to the low frequency range of the acoustic spectrum with two instruments: GOLF, Global Oscillations at Low Frequency described by Gabriel et al. (1995) and MDI, a Michelson Doppler Imager built by Scherrer et al. (1995). This part of the spectrum, contrary to the high frequency range, is not sensitive to the variability of the subsurface layers along the solar cycle (Turck-Chièze et al. 2001b; Couvidat et al. 2003b). The corresponding modes have longer lifetimes but smaller intensities (Bertello et al. 2000; García et al. 2001). From these observations, a very clean sound speed profile has been established down to 0.06 $R_\odot$ together with a reasonable density profile. It has been compared to the theoretical models for different solar compositions. For the latest sets of solar abundances with lowered oxygen abundance (Holweger 2001; Asplund et al. 2009; Caffau et al. 2008), the theoretical profiles show clear differences compared to the observed sound speed, that still need to be understood (Turck-Chièze et al. 2001b, 2004a).

2.1.1. The Nuclear Processes

It is interesting to notice that each physical ingredient of the structural equations (specific nuclear rate, specific opacity coefficient, screening or Maxwellian tail distribution) has a specific signature on the sound speed profile (Turck-Chièze et al. 1997). It has thus been of prime importance to check the validity of the involved nuclear processes. Turck-Chièze et al. (2001a) note that the present sound speed profile does not favor any tiny variation of the Maxwellian distribution of the ions nor strong screening or large mixing in the core. The core sound speed profile and the specific signature of the pp reaction rate put strong observational constraints on the cross section at a level of 1% including the screening effect. This cross section is known only theoretically due to the weak character of the interaction. The other nuclear cross sections have been measured in laboratory during the last three decades but the extrapolation toward the stellar plasma conditions has been only measured for the (^{3}He, ^{3}He) interaction.

At present, the reaction rates are generally considered to be reasonably well under control, and in the CESAM code in particular, we use the most recent estimates for the ^{7}Be$(p,\gamma)^8$B (Junghans et al. 2005)[5] and ^{14}N(p, γ)^{15}O (Formicola et al. 2004). That last cross section leads to a consequent reduction of the CNO contribution to the nuclear energy in main sequence. Some uncertainties could remain on the screening effect of CNO processes but they play a rather small role in the present confrontation of the models to the two mentioned probes. Tables 1 and 2 summarize our previous and present works. For a comparison between the values of Table 1 and the work of Bahcall and collaborators over the years, the reader is referred to Turck-Chièze (2004). Table 2 takes into account the neutrino oscillations determined by $\Delta m^2_{12} = 7 \times 10^{-5}$ eV^2 and $tg^2\theta_{12} = 0.45$ recommended by Bahcall & Pena-Garay (2004); these values are compatible with the most recent estimates within the error bars.

[5] The astrophysical S-factor determined by Junghans et al. (2005) is $S_{17}(0) = 21.4 \pm 0.5\,(\text{stat}) \pm 0.6\,(\text{syst})$. Some slightly higher values are discussed by Igamov & Yarmukhamedov (2008).

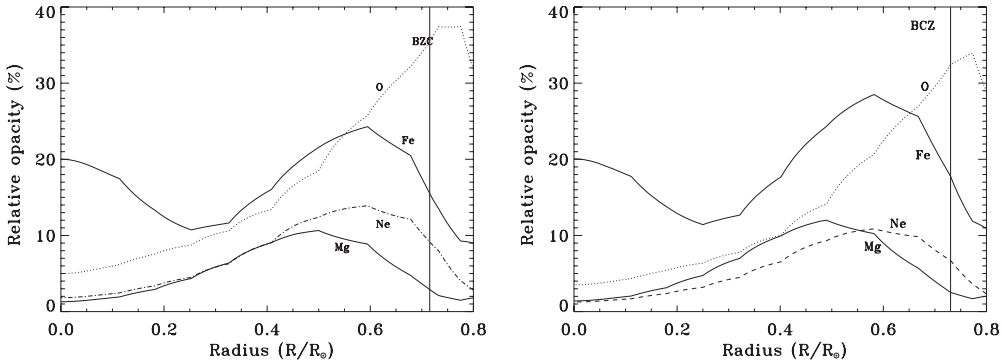

Figure 1. Relative contribution of the most important heavy element contributors to the total opacity when one considers the solar composition proposed by Grevesse & Noels (1993) (left) and Asplund et al. (2004) (right). An intermediate value of the oxygen contribution is now more compatible with the recent studies (Asplund et al. 2009; Caffau et al. 2008, 2009). We have noticed that slight differences exist between the different opacity tables due to slightly different states of ionization of the different species (Turck-Chièze et al. 2009).

Table 2
Comparison of the Solar Seismic Model Predictions and the Detection of the Different Neutrinos

SNO predictions: $5.31 \pm 0.6 \times 10^6$ cm^{-2} s^{-1}
SNO results: 5.21 ± 0.27 (stat) ± 0.38 (syst) 10^6 cm^{-2} s^{-1}
Gallium prediction without neutrino oscillations: 123.4 ± 8.2 SNU
Gallium prediction with neutrino oscillations: 66.65 ± 4.4 SNU
Gallium detection: GNO+Gallex: $70.8 \pm 4.5 \pm 3.8$ SNU; SAGE: $70.8 \pm 5.3 \pm 3.7$ SNU
Chlorine prediction without neutrino oscillations: 7.6 ± 1.1 SNU
Chlorine prediction with neutrino oscillations: 2.56 ± 0.23 SNU
Chlorine detection: 2.56 ± 0.16(stat) ± 0.16(syst) SNU
^{7}Be prediction without neutrino oscillations: 4.72×10^9 cm^{-2} s^{-1}
^{7}Be prediction with neutrino oscillations: 3.045×10^9 cm^{-2} s^{-1}
BOREXINO detection: 49 ± 3 (stat) ± 4 (sys) counts/day/100 tons or $3.36 \pm 0.365 \times 10^9$ cm^{-2} s^{-1}

2.1.2. The Impact of the Solar Composition on the Radiative Zone Properties

One important question has emerged from the new spectroscopic estimates of the carbon, nitrogen, and oxygen atmospheric abundances, leading to a reduction by 20%–30% of the related abundances: "Are we so sure that we understand properly the inner composition of the Sun in the radiative zone"? This question is an important issue because the solar abundance is chosen as a reference for the stellar evolution models. For instance, up until recently, the abundance of these nuclides was larger than that of any other heavy element by about a factor 10 in Population II stars, so the change in the solar CNO abundance has a strong impact on the evaluation of their chemical pattern (Turck-Chièze et al. 2004a). The situation is now clarified because the three independent analyses (Holweger 2001; Asplund et al. 2009; Caffau et al. 2008) converge to about the same reduction. A reduction by a similar factor (30%) of the iron content also appeared in the early nineties, but with rather small effects on the whole radiative zone (Turck-Chièze & Lopes 1993).

As far as CNO elements are concerned, this substantial reduction has a real impact on the radiative sound speed profile mainly due to the subsequent change in the oxygen opacity (see Figure 1) and modifies the depth of the convective envelope (Turck-Chièze et al. 2004a; Bahcall et al. 2005). The confrontation between helioseismic indicators and results of SSMs was examined extensively (Turck-Chièze et al. 2004a; Bahcall et al. 2005, Guzik et al. 2005). It is frustrating to note that the sound speed and density profiles of the model including the updated solar chemical composition are very similar to those corresponding to the case where we omitted to account for the slow gravitational settling of the nuclides (Thoul et al. 1994; Brun et al. 1998) and that this last update destroys the apparent agreement with the observed one. We may thus quantify the effect of the change of composition since the inclusion of the microscopic processes corresponds to a reduction by 10%–12% of all the heavy elements. Consequently a 20% variation of CNO abundances is almost equivalent to the 7%–9 % variation of all the heavy elements due to gravitational settling, or to an equivalent change of opacity coefficients if all the elements were concerned. See Turck-Chièze et al. (1997) where the impact of a lot of changes is considered and Table 1 for the consequence on neutrino predictions.

Effectively, a change in the CNO abundances also affects the mean total opacity of the stellar plasma, and thus the evolution of the Sun up to its present status as well as its present structure. The knowledge of the opacity coefficients used in a solar model is up to now purely theoretical. The conditions of temperature and density in the radiative zone ensure that the plasma is only fully ionized for its main constituents, hydrogen and helium, but heavier species such as iron down to oxygen become partially ionized in the radiative zone as summarized in Figure 1. It is why the bound–bound and the bound–free interactions of photons with matter limit the evacuation of the energy produced within the inner 25% of the radius, corresponding to half the solar mass (Iglesias & Rogers 1996). The small amount of iron (only 2.8×10^{-5} of the hydrogen contribution in fraction number) contributes to about one-fifth of the opacity cross section in central conditions (see Figure 1 and Turck-Chièze et al. 1993 for more details). The oxygen is the second contributor and plays a crucial role in determining the base of the convective zone.

Up until now the details of the ion interactions have been verified only indirectly through acoustic pulsation eigenmodes.

These modes probe plasma properties throughout the Sun from 6% $R_\odot$ up to the limit of the convective zone. However, they depend on both the detailed composition and opacity. To disentangle both contributions would require a high radial resolution of the seismic data allowing us to capture some specific bound–bound effect through bumps in the radial sound speed profile in the radiative zone (Turck-Chieze 1998) that is still out of reach at present.

Some proposed solutions to reconcile the standard model with revised CNO abundances and helioseismology (Guzik et al. 2005; Lin et al. 2007; Basu & Antia 2008) have not been retained. Some others seem to favor the old composition (Basu et al. 2007; Serenelli et al. 2009). We explore, here, the idea that the SSM framework is questionable. Considering that any improvement has always been considered like a new informative fact and that a better determination of CNO has been awaited since the nineties (Turck-Chièze et al. 1993), the present facts suggest three reasonable solutions which could all exist simultaneously:

1. The gravitational settling is not well constrained today for CNO and heavy elements. The photospheric helium content deduced from helioseismology (Vorontsov et al. 1991) of $Y = 0.25 \pm 0.03$ (and confirmed by Basu 1995) for OPAL equation of state (EOS) has confirmed the need to take into account this slow atomic diffusion introduced first by Cox et al. (1989). This process leads today to a reduction of about 10%–15% of the He mass fraction at the solar surface (Christensen-Dalsgaard et al. 1993; Thoul et al. 1994; Brun et al. 1998; Michaud 2004) but we cannot check yet if the order of magnitude is correct also for CNO and iron.
2. The opacity coefficients used in the models have never been verified by laboratory measurements under the physical conditions of the stellar interiors and may be a source of uncertainty. The high energy lasers developed in France (LIL, LMJ) and in the United States (NIF) will offer conditions corresponding to the solar radiative zone and might help in constraining these quantities. We are preparing experiments to measure the absorption energy spectrum of isolated elements and mixtures in plasma conditions which are more and more useful for the stellar community (Bailey et al. 2007; Loisel et al. 2009; Turck-Chièze et al. 2009). Laboratory opacity and EOS experiments might benefit in the coming decade from an equivalent effort to the one dedicated to nuclear reaction rate measurements. A detailed verification of the interaction between photons and plasma will contribute to disentangle the different processes in the deep interior of stars.
3. The radiative zone of the Sun is not well reproduced by the hypotheses of the SSM, and we need to improve the models by the addition of dynamical processes. It is one of the reasons to develop the DSM which must introduce the dynamics of the tachocline, the gravity waves generated at the base of the convective envelope and propagating in the radiative interior, the presence of a potential magnetic field, and the different transport processes induced by the rotation. Guzik & Mussak (2010) examine the idea of mass loss and accretion, and in a coming work, we question the hypothesis of the energetic balance (Turck-Chièze et al. 2010).

Such a complete model of the Sun is not ready to be compared to seismic and neutrino probes; it is why we have developed an intermediate model, the seismic model described in the following section. A first step toward the DSM is then to confront all the probes with solar models including rotation, which is the purpose of the present paper. We shall produce models in the following sections which can be considered as the DSM1 step.

2.2. Prediction of Neutrino Fluxes, Gravity Mode Frequencies and Structural Profiles from SSeM

The quality of the seismic observations is such that one can build a seismic model. This model is designed to reproduce the measured solar sound speed using the classical stellar evolution equations and slightly changing some recommended specific absolute values of physical inputs within their own uncertainties (Turck-Chièze et al. 2001b, 2004a; Couvidat et al. 2003a). It can be established for the new solar composition and will converge to the same predictions by definition.

The interest of such a model comes from the idea that the standard framework is obviously too crude to reproduce all the existing observed quantities. This model is useful to improve the prediction of the neutrino fluxes (Tables 1 and 2) or the gravity mode frequencies because it implicitly includes the known sound speed profile (Turck-Chièze et al. 2004a; Couvidat et al. 2003a; Mathur et al. 2007).

Table 1 illustrates the time evolution of the predicted ^{8}B neutrino flux which depends strongly on the central temperature and consequently, on the details of the plasma properties. The seismic model prediction (Turck-Chièze et al. 2001b; Couvidat et al. 2003a) agrees remarkably well with the measured value obtained with the SNO detector (filled with heavy water), which is sensitive to all the neutrino flavors (Ahmed et al. 2004). For the gallium or water detector predictions, one needs to inject the energy dependent reduction factor due to the fact that the electronic neutrinos are partially transformed into muon or tau neutrinos. This property of neutrinos was confirmed last year by the Borexino results (Arpesella et al. 2008). Doing so, the agreement between the predictions of the seismic model and all the detectors is extremely good (Turck-Chièze et al. 2005). Table 2 confirms that it is also true for the beryllium neutrinos.

Another interesting property of the SSeM is the fundamental periodicity P_0 which characterizes the asymptotic behavior of the gravity modes nearly equally spaced in period for frequencies below $\sim$100 μHz. $P_0 = 2\pi^2 \left(\int_0^{r_c} \frac{N}{r} dr\right)^{-1}$ where N is the Brunt-Väisälä frequency and r_c is the radius at the convective bottom. Before the launch of *SoHO*, there was a great dispersion in the theoretical predicted values of P_0. Following Hill et al. (1991), its value was varying from 29 minutes to 63 minutes depending on the models. Today, standard and seismic models agree within one minute, which helps to predict the general properties of the gravity modes (Mathur et al. 2007) because models have been improved by the understanding of the property of the modes and their sensitivity. Nevertheless the present standard model, including the new CNO composition, largely deviates from the seismic observations; consequently, the value of P_0 might be better determined by the seismic model or any coming model in agreement with seismic observations. Of course, the detection of individual gravity modes might improved the density profile in the core and consequently will put more pressure on the seismic model in the core.

Despite the remarkable agreement between the two probes of the central region of the Sun (neutrinos and helioseismology), SSeM is not a physical model and SSM predictions with the new solar composition encounter a series of difficulties. In the following section, we present a first step to transform SSM or SSeM into a more realistic DSM1, by introducing rotation and

the associated transport of matter and angular momentum in the computations.

3. HOW TO MODEL THE INTERNAL ROTATION IN ONE–DIMENSIONAL STELLAR EVOLUTION CODES

3.1. Meridional Circulation and Shear-induced Turbulence: Adopted Formalism

The present Sun is a slowly rotating star ($\simeq$2.2 km s^{-1} at the equator, 1.7 km s^{-1} near the poles). It is thus a reasonable first-order approximation to treat rotation with a perturbative approach and to adopt the hypothesis of spherical symmetry in the standard model framework. We may nevertheless recall that the solar superficial deformations can be measured and that the quadrupolar moment is of the order of 1.84×10^{-7} (Lydon & Sofia 1995) and will be improved by the microsatellite PICARD (Thuillier 2005).

Even if departures from spherical symmetry can be considered small in the solar case, they are sufficient for rotation to induce large-scale circulations in the radiative and convective interior, that will simultaneously advect angular momentum, and chemical species (Busse 1982; Zahn 1992). Moreover, in case of radial differential rotation, which could be the case in the solar deepest interior, different hydrodynamical instabilities may develop that will generate hydrodynamical turbulence in the radiative regions. Laboratory Couette–Taylor experiments conducted for Reynolds numbers Re $\simeq 10^6$ by Richard & Zahn (1999) indicate the development of turbulence in the flows. This gives a good hint that in stellar interiors, where the typical Reynolds number is of about 10^{12} (solar case), the hydrodynamical instabilities associated with differential rotation eventually become turbulent.

Following Zahn (1992), Maeder & Zahn (1998), and Mathis & Zahn (2004), the transport of angular momentum and chemical species by meridional circulation and shear-induced turbulence has been added to the stellar structure equations in order to estimate the effects of such a transport on the evolution and the structure of the Sun up to the present time.

Under the assumption of shellular rotation ensured by a strong anisotropy of the turbulent diffusivities $D_h \gg D_v$, all the relevant variables and vectorial fields may be described as the sum of the mean value over an isobar and of a second (or fourth) order perturbation (Zahn 1992; Mathis & Zahn 2004). This means that the variables are projected on a basis of Legendre polynomials, an approach very similar to that used in helioseismology. This allows us to separate angular and radial parts and thus to account for the rotational transport of angular momentum and chemicals over secular timescales in one-dimensional stellar evolution codes, while two-dimensional or three-dimensional secular stellar evolution is still far from maturity.

Using this formalism, the momentum equation

$$\rho\left[\frac{\partial \vec{V}}{\partial t} + (\vec{V}.\vec{\nabla})\vec{V}\right] = -\vec{\nabla}P - \vec{\nabla}\phi + \vec{\nabla}.||\tau|| \qquad (1)$$

becomes, when averaging over the isobar and using an azimuthal projection:

$$\rho\frac{d}{dt}(r^2\overline{\Omega}) = \frac{1}{5r^2}\frac{\partial}{\partial r}(\rho r^4\overline{\Omega}U_2) + \frac{1}{r^2}\frac{\partial}{\partial r}\left(\rho\nu_v r^4\frac{\partial\overline{\Omega}}{\partial r}\right), \qquad (2)$$

where $\overline{\Omega} = \Omega(r)$ is the mean angular velocity on the isobar of radius r and ν_v is the vertical turbulent viscosity associated to the shear instability (see Equation (8)).

U_2 is the vertical meridional velocity component:

$$U_2 = \frac{P}{\rho g C_p T[\nabla_{\rm ad} - \nabla + (\phi/\delta)\nabla_\mu]}\left(\frac{L}{M_\star}(E_\Omega + E_\mu)\right), \qquad (3)$$

with P is the pressure, C_p is the specific heat, E_Ω and E_μ are terms depending on the Ω- and μ-distributions respectively, up to the third-order derivatives and on various thermodynamic quantities (see details in Maeder & Zahn 1998).

Equation (2) is split into a system of four first-order equations in Ω complemented by an equation describing the evolution of the horizontal mean molecular weight fluctuations due to the vertical μ gradient for a given horizontal turbulence and a vertical velocity:

$$\frac{d\Lambda}{dt} + U_2(r)\frac{\partial \ln\overline{\mu}}{\partial r} = -6D_h\Lambda, \qquad (4)$$

where $\Lambda = \frac{\tilde{\mu}}{\mu}$ and D_h is the horizontal turbulent diffusivity.

The equation for the transport of nuclides by meridional circulation and shear-induced turbulence can be written as a diffusion equation (see, e.g., Chaboyer & Zahn 1992):

$$\left(\frac{dX_i}{dt}\right)_{M_r} = \frac{\partial}{\partial M_r}\left[(4\pi r^2\rho)^2(D_v + D_{\rm eff})\frac{\partial X_i}{\partial M_r}\right] + \left(\frac{dX_i}{dt}\right)_{\rm nucl} + \left(\frac{dX_i}{dt}\right)_{\rm micro}, \qquad (5)$$

where X_i is the mass fraction of the ith nuclide, the second and third terms are, respectively, the nuclear (nucl) and gravitational settling (micro) terms. $D_v \equiv \nu_v$ is the vertical component of the turbulent diffusivity. $D_{\rm eff}$ is the diffusion coefficient associated to the action of the meridional circulation, and it is given by

$$D_{\rm eff} = \frac{(rU_2)^2}{30D_h}. \qquad (6)$$

These transport equations have to be solved at each evolutionary time step, adding a set of five coupled nonlinear equations to the usual set of structure equations. This explains the small number of stellar evolution codes including this treatment: the STAREVOL code (Palacios et al. 2006) and the Geneva stellar evolution code (Eggenberger et al. 2008). It has been recently included in the CESAM stellar evolution code.

Following the effects of rotation according to the above described formalism is even more difficult in the solar case due to the small perturbation they cause on the solar structure. In order to test the quality of our results, we have decided to confront the results obtained with two different stellar evolution codes using distinct numerical approaches. We have computed rotating solar models with both STAREVOL and CESAM codes. In the following, we present the codes, the numerical implementation of the Maeder & Zahn formalism, and the main characteristics of the solar models that will be discussed in the forthcoming sections.

3.2. Stellar Evolution Codes

3.2.1. CESAM

The CESAM code has been developed by a consortium of French astrophysicists to get a stellar evolution code of

high accuracy for numerous seismic uses. This code is robust and used by a large international community. It is free of access for basic use (http://www.oca.eu/cesam), which means standard physics excluding the dynamical processes. Details of the code are described in Morel (1997). This code does not use the natural variables to avoid the singularities at the center. Moreover, CESAM does not solve the nonlinear problem of the limited conditions in the physical space but in the B-splines space. This allows a good continuity of the functions and their derivatives. In fact, this code has been specially built for a helio and asteroseismic perspective, so all the variables used to calculate the frequencies of the acoustic and gravity modes are correctly calculated. The treatment of the transport equations by rotation has been recently improved by Marques (2010); it is now done in the physical space with a projection of the quantities, associated to the rotation, on the vectorial spherical harmonics. These equations are solved independently of the structural equations, and then all the interpolations from one model to the next one (in time) are done on the B-spline basis.

CESAM has been used by our team since 1995 (see the references in Table 1), in place of the Paczynski BINARY code used in the 1980s for the predictions of helio and asteroseismic probes and for neutrinos. With time, the code has been enriched by the different updated pp and CNO cross sections of the hydrogen burning. For the Sun, we use the recommended values of the Seattle meeting (Adelberger et al. 1998), then the most recent updates quoted in Section 2. We have included the appropriate screening and use the Mitler prescription (Dzitko et al. 1995) and the microscopic diffusion described in Brun et al. (1998). CESAM is regularly updated with the most recent EOS and opacity coefficients (Iglesias & Rogers 1996; Iglesias & Rose 1996). It included the different updates on the solar composition with an adapted low-temperature opacity table (Turck-Chièze et al. 2004a). The models of this paper use the Holf atmosphere (see the difference between Kurucz and Holf atmosphere in Couvidat et al. 2003a).

For a comparison with the STAREVOL code, we have used the Grevesse & Noels (1993) composition. This choice has no bearing on the results because we show mainly relative comparison and because the solar structure is only slightly modified by the effects of rotation.

3.2.2. STAREVOL

The code STAREVOL has been applied to model stars all over the H-R diagram, and more specifically to study the effect of dynamical processes on stellar evolution and nucleosynthesis (Palacios et al. 2003, 2006; Charbonnel & Talon 2005; Decressin & Charbonnel 2005; Decressin et al. 2009). Let us briefly recall here the main ingredients used for the computation of the solar model. We use Grevesse & Noels (1993) as reference for the solar chemical composition. The nuclear network includes 52 species up to ^{37}Cl. The associated nuclear reaction rates for charged and neutron particle captures as well as beta decays have been kept up-to-date using the NETwork GENerator tool available at http://astropc0.ulb.ac.be (see Siess 2006 for details). At low-temperature ($T < 8000$ K), the atomic and molecular opacities are given by Alexander & Ferguson (1994). Between $8000 \leqslant T \leqslant 5 \times 10^8$ K, we use the OPAL tables (Iglesias & Rogers 1996). The neutrino energy loss rates are computed according to Itoh et al. (1996) and take into account the effects of plasma, pair, bremsstrahlung, recombination, and photo neutrino emission.

Table 3
Characteristics of the Rotating Solar Models Computed With CESAM (A_C, B_C) and STAREVOL (A_S, A'_S, B_S, C_S) Codes

Model	D_h	$J_{\rm initial}$	$\upsilon_{\rm ZAMS}$	$\upsilon_{\odot}$
A_C	Mathis et al. (2004)	3.27×10^{48}	2.19 km s^{-1}	2.13 km s^{-1}
A_S	Mathis et al. (2004)	4.84×10^{48}	2.15 km s^{-1}	2.05 km s^{-1}
A'_S	Zahn (1992)	4.84×10^{48}	2.15 km s^{-1}	2.03 km s^{-1}
B_C	Mathis et al. (2004)	1.10×10^{49}	19.6 km s^{-1}	2.09 km s^{-1}
B_S	Mathis et al. (2004)	3.88×10^{49}	19.7 km s^{-1}	3.08 km s^{-1}
C_S	Mathis et al. (2004)	8.74×10^{49}	53.2 km s^{-1}	3.03 km s^{-1}

Notes. All STAREVOL models were computed using $\alpha_{\rm MLT} = 1.7378$ and initial helium mass fraction $Y_{\rm ini} = 0.280$. In this study, only the CESAM models are calibrated in luminosity and radius at the present age.

The EOS is based on the principle of Helmholtz free energy minimization and is described in detail in Siess et al. (2000). The atmosphere is treated in the gray approximation and integrated up to an optical depth $\tau \simeq 5 \times 10^{-3}$. Convection is modeled following the mixing length formalism, and a common parameter $\alpha_{\rm MLT} = 1.7378$ has been adopted for the three models presented here, ensuring that the solar luminosity and radius are reproduced with at most 0.1% error (see Table 6). We apply the Schwarzschild criterion for the convective instability. Convective regions are assumed to undergo instantaneous mixing of chemicals and to rotate as rigid bodies. For the solar model, mass loss was not taken into account. The Maeder & Zahn (1998) formalism is applied, and the resulting set of five nonlinear differential equations is solved using a Newton–Raphson numerical scheme according to Henyey et al. (1964) as described in Palacios et al. (2006). The transport of nuclides by gravitational settling is also accounted for in all the rotating solar models. It is introduced using the approximation of Paquette et al. (1986) for the microscopic diffusion coefficient and the expressions given by Montmerle & Michaud (1976) for the microscopic diffusion velocity.

3.3. Assumptions Introduced in the Rotating Models of the Sun

The Sun is the only star where we can perform quantitative comparison of the impact of the above prescriptions on the sound speed and the rotation profiles which can now be deduced from helioseismic data. So, it is interesting to discuss in details the role of the different terms and the choice for the prescriptions. In the following section, we shall present two types of models: one model with an extremely slow initial rotation which does not justify external magnetic braking (A or *slow* models), and two models with greater initial rotation and magnetic braking at the surface (models B and C, or *intermediate* and *strong* rotation models). The main characteristics of these models are given in Table 3. These cases allow us to discuss the order of magnitude of the meridional circulation, the diffusion coefficients, and the gradient of the internal angular velocity profile, together with their different roles in the building of the present solar rotation profile.

For these models, we have adopted the Mathis et al. (2004) prescription for the horizontal component of the turbulent diffusivity D_h:

$$D_h = \sqrt{\left(\frac{\beta}{10}\right)(r^2\overline{\Omega})\,[r|2V_2 - \alpha U_2|]}. \quad (7)$$

The vertical component of the turbulent diffusivity D_v is from

Table 4
Characteristics of the Models Computed with CESAM for the Slow Initial Rotation

Age (Gyr)	R ($R_\odot$)	L ($L_\odot$)	E_G (%)	E_{pp} (%)	E_{CNO} (%)	T_c	ρ_c	$\upsilon_{c,eq}$ (km s^{-1})	υ_s (km s^{-1})
0	17.2	73.0	100	0	0	4.83×10^5	2.1×10^{-3}	0.08	0.08
0.00001	10.5	32.9	100	0	0	7.69×10^5	8.5×10^{-3}		0.12
0.0001	4.90	8.7	100	0	0	1.6×10^6	7.8×10^{-2}		0.25
0.001	2.20	1.8	100	0	0	3.53×10^6	8.2×10^{-1}		0.55
0.015	1.12	0.46	100	0	0	6.67×10^6	1.23×10^1	2.41	1.18
0.020	1.02	0.63	94	6	0	9.26×10^6	4.39×10^1		1.64
0.030	0.96	0.89	33	65	0	1.32×10^7	8.01×10^1		2.06
0.039	0.88	0.71	33	92	8	1.36×10^7	7.88×10^1		2.19
0.050	0.87	0.70	0	94	6	13.5×10^6	7.89×10^1	5.03	2.18
0.147	0.88	0.72	0	98	2	13.5×10^6	8.26×10^1		2.18
1	0.9	0.77	0	100	0	13.8×10^6	91.2	5.6	2.177
2	0.923	0.82	0	100	0	14.2×10^6	102.6	6.1	2.17
3	0.948	0.88	0	100	0	14.7×10^6	111.7	6.3	2.16
4.6	0.997	1.003	0	99	1	15.65×10^6	147.4	8.2	2.13

Talon & Zahn (1997):

$$D_v = \frac{Ri_c}{N_T^2/(K_T + D_h) + N_\mu^2/D_h}(r\partial_r\overline{\Omega})^2 \quad (8)$$

with $Ri_c = 1/6$ the critical Richardson number, K_T is the thermal diffusivity, N_T and N_μ are the chemical and thermal parts of the Brunt-Väisälä frequency $N^2 = N_T^2 + N_\mu^2$.

Referring back to Talon & Zahn (1997), let us recall here that for the shear instability to develop, not only the Richardson criterion must be satisfied, but the sheared flow shall be turbulent. This is controlled by the Reynolds criterion. In our models, we used a critical Reynolds number $\mathrm{Re}_c = 10\nu_{\mathrm{mol}}$. When $\nu_v < \mathrm{Re}_c$, D_v is replaced by ν_{mol} in the transport equations for angular momentum and nuclides.

The choice of slow and mild rotators on the zero age main sequence (hereafter ZAMS) refers to the two identified populations of young stars as pinpointed by Bouvier (2009): the slow rotators for which the angular momentum evolves like Ω^3 and the fast rotators for which the angular momentum varies like Ω.

The A models explore the extreme case of slow rotators on the pre-main sequence (hereafter PMS) and on the ZAMS, with a surface equatorial velocity of about 2.2 km s^{-1} remaining almost constant from the ZAMS to the present age of the Sun. No braking is applied at the surface. These models do not actually reproduce observed stars, and can be considered more as academic cases used to show the respective impact of the meridional circulation and shear turbulence on the shape of the angular velocity profile even with such small velocities. They are also used to estimate interesting quantities relevant for the present observations.

The B and C models are mild rotators at their arrival on the ZAMS (approximately 20 km s^{-1} and 50 km s^{-1}, respectively). These models undergo magnetic braking at the arrival on the main sequence, similar to the solar-mass models by Talon & Charbonnel (2005).

Rotation is included from the PMS in all our models. We assume solid-body rotation as the initial state in the completely convective PMS star. When magnetic braking is applied at the arrival on the main sequence, we use the formalism developed by Kawaler (1988; see also Bouvier et al. 1997; Palacios et al. 2003) in order to obtain the solar surface equatorial velocity when the model reaches 4.6 Gyr:

$$\left(\frac{dJ}{dt}\right) = -K\Omega^3\left(\frac{R}{R_\odot}\right)^{1/2}\left(\frac{M}{M_\odot}\right)^{-1/2} \quad (\Omega < \Omega_{\mathrm{sat}}), \quad (9)$$

$$\left(\frac{dJ}{dt}\right) = -K\Omega\Omega_{\mathrm{sat}}^2\left(\frac{R}{R_\odot}\right)^{1/2}\left(\frac{M}{M_\odot}\right)^{-1/2} \quad (\Omega \geqslant \Omega_{\mathrm{sat}}). \quad (10)$$

This formulation corresponds to a field geometry intermediate between a dipolar and a radial field (Kawaler 1988), and it is widely used in the literature (Chaboyer et al. 1995; Krishnamurthi et al. 1997; Bouvier et al. 1997; Sills et al. 2000). The parameter K in Kawaler's law is related to the magnitude of the magnetic field strength, and is adjusted accordingly with the adopted initial rotation velocity. Ω_{sat} expresses the fact that the magnetic field generation saturates beyond a certain evolutionary point. This saturation is actually required in order to retain a sufficient amount of fast rotators in young clusters, as originally suggested by Stauffer et al. (1987). Here, we adopt $\Omega_{\mathrm{sat}} = 14\Omega_\odot$ following Bouvier et al. (1997). Table 3 presents the main characteristics of models A, B, and C computed with STAREVOL and CESAM.

4. THE ROTATING SOLAR MODELS AND THEIR SENSITIVITY TO THE PRESCRIPTIONS USED

The computation of solar rotating models is tricky due to the subtle changes induced by rotational mixing on the internal structure of the Sun. The aforementioned formalism being newly introduced in the CESAM code, we compare first in this section the results obtained with STAREVOL and CESAM in order to achieve a mutual validation of the results. The numerical approach to solve the stellar structure equations in CESAM and STAREVOL is significantly different and also is the numerical implementation of the transport of angular momentum equation. We thus do not expect a perfect match between the rotating solar models computed with each code, but orders of magnitudes and shapes for the different profiles are expected to be similar.

4.1. An Extreme Case: The Sun, a Slow Rotator on the ZAMS

We consider first the extreme case where the initial angular momentum is small so that the model arrives on the ZAMS as a slow rotator ($\upsilon_{\mathrm{ZAMS}} \approx 2.2$ km s^{-1}) without undergoing any magnetic braking.

Table 4 shows the evolution of several quantities, among them the surface velocity in the center and at the surface of model

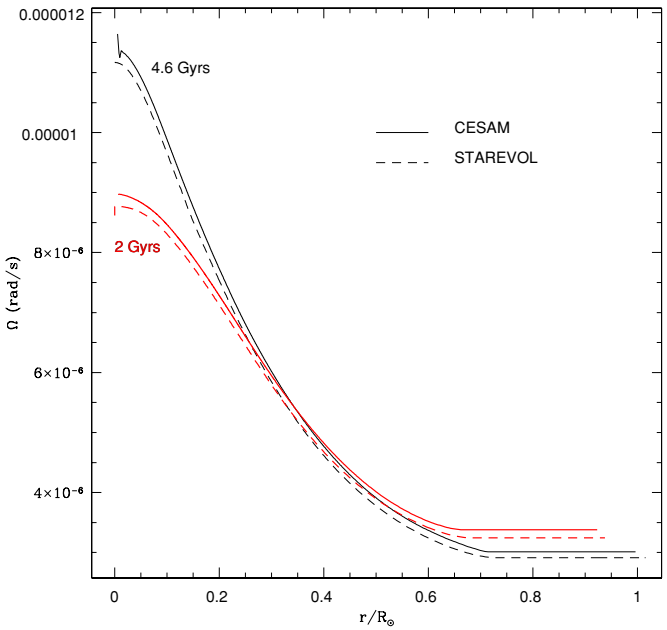

Figure 2. Comparison of angular velocity profiles between the two codes CESAM (C) and STAREVOL (S) for slow rotating models A_C (solid lines) and A_S (dashed lines) at 2 Gyr and 4.6 Gyr.

(A color version of this figure is available in the online journal.)

A_C. With an initial rotation of about 0.1 km s^{-1}, the surface velocity is seen to increase to reach 2.19 km s^{-1} at the arrival on the ZAMS ($t = 390$ Myr), and then remains almost constant up to the present age of the Sun. In the central regions, the increase of the rotation velocity is maintained during the main sequence, so that at the present age, υ_C is about 4 times larger than υ_S. This velocity gradient clearly appears in Figure 2 and on the left panel of Figure 7, where the evolution of the angular velocity Ω is displayed for models A_C and A_S. We may note here the very good agreement between the profiles obtained with CESAM and STAREVOL for solar models calibrated within 1%, thus validating the numerics of both codes. The building of the Ω-gradient is due on the PMS to the rapid contraction of the central regions when radiation becomes the dominant energy transport process in the core, as well as to the combined effects of meridional circulation and shear-induced turbulence.

Despite the very slow rotation of these models, a small temperature gradient is generated between the pole and the equator and a meridional circulation develops in the radiative interior. The velocity of the meridional currents, U_2, is of the order of 10^{-9} cm s^{-1} in absolute value at 4.6 Gyr as can be seen in Figure 3, left. This flow is extremely small compared to the meridional circulation in the convective zone. The circulation consists in a single counterclockwise loop, e.g., U_2 negative. The flow is directed downward, peaking near the base of the convective zone, extracting angular momentum from the central region to the base of the convective envelope. The profiles obtained with both codes are of similar shape and amplitude. They present irregularities mainly due to the mean molecular weight variations $\Lambda = \frac{\tilde{\mu}}{\mu}$ that introduce nonlinearities in the system because some noise is coming from the mean molecular weight gradient. Let us here recall that the transport of angular momentum introduced in the codes is treated in a self-consistent but simplified manner. Such models give hints, order of magnitudes, and global shapes, but should not be expected to deliver exact profiles.

The diffusion coefficient profiles are also similar in the two codes (see Figure 4, left). The effective diffusion coefficient $D_{\rm eff}$ is proportional to $(U_2)^2/D_h$ and consequently is very small (about 10^{-5}–10^{-3} cm^2 s^{-1}) due to the slow meridional circulation velocity and the large horizontal component of the turbulent diffusivity ensured by the use of the Mathis et al. (2004) prescription. The Reynolds number of the sheared flow is lower than the critical Reynolds number $\mathrm{Re}_c \propto 10\nu_{\rm mol}$ in the bulk of the radiative zone. The flow is not turbulent, so the vertical component of the turbulent diffusivity D_v is essentially set equal to the local molecular viscosity (see Section 3.3). The effective diffusion coefficient is actually much smaller than the microscopic diffusivity (see, e.g., Brun et al. 1999), which is of the order of 10 cm^2 s^{-1} in solar models. Consequently, the microscopic diffusion is the most efficient process to transport

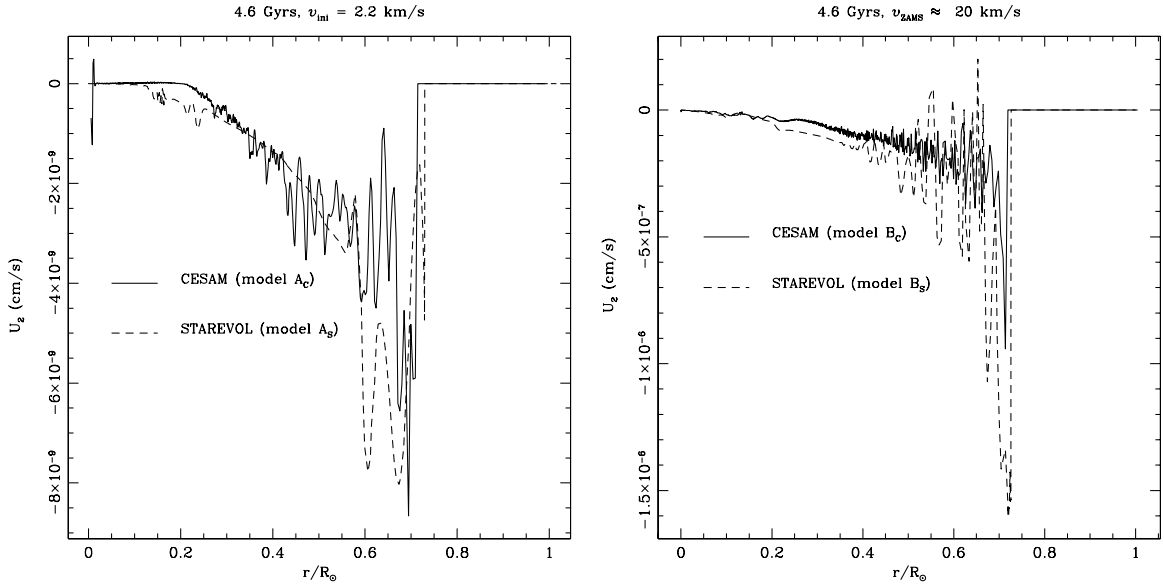

Figure 3. Meridional circulation velocity profiles for solar models at 4.6 Gyr computed with CESAM (solid lines) and STAREVOL (dashed lines) for very slow initial rotation (left) and mild initial rotation (right).

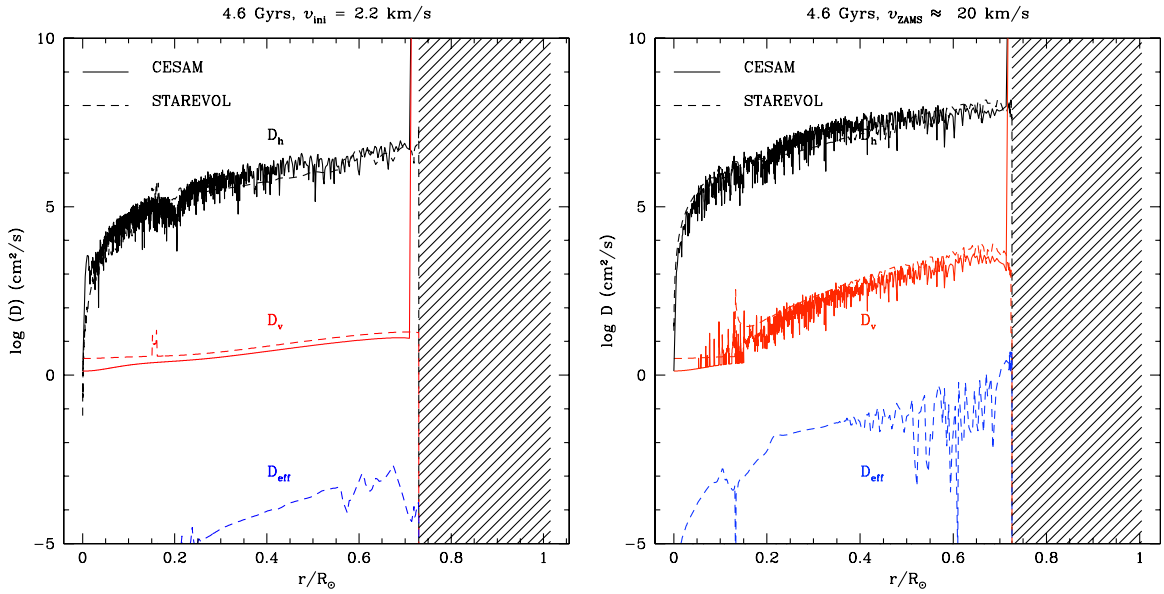

Figure 4. Diffusion coefficient profiles for solar models at 4.6 Gyr computed with CESAM and STAREVOL. The horizontal turbulent diffusion coefficient D_h, the vertical turbulent diffusion coefficient D_v, and the effective diffusion coefficient $D_{\rm eff}$ are presented for models A_C (solid) and A_S (dashed) on the left panel and for models B_C (solid) and B_S (dashed) on the right panel.

(A color version of this figure is available in the online journal.)

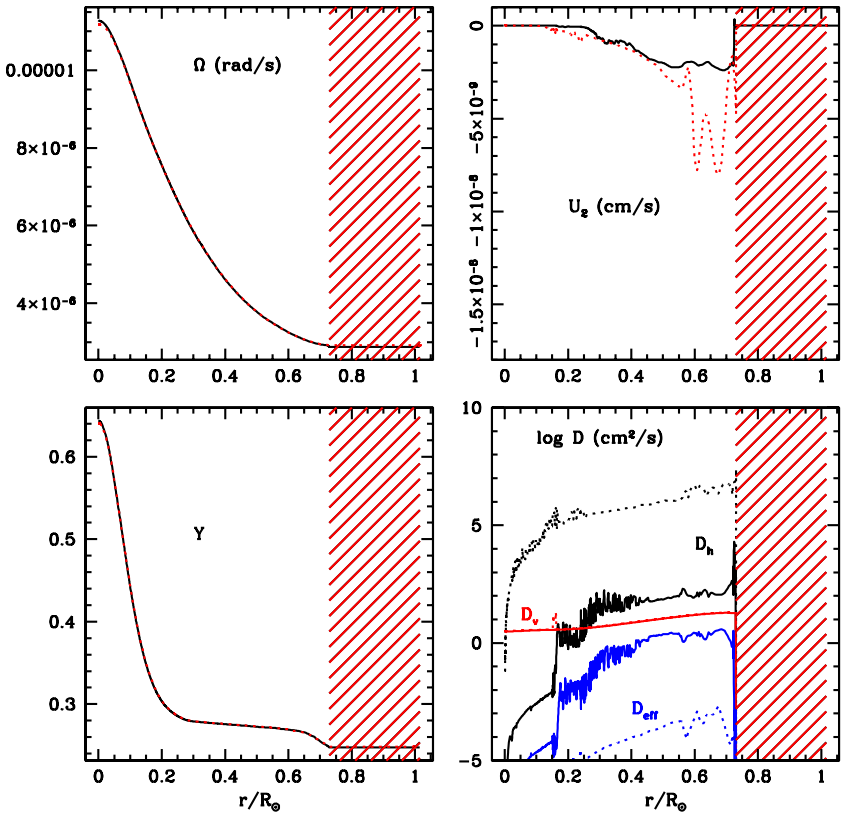

Figure 5. Profiles of the angular velocity Ω, the meridional circulation velocity U_2, the helium mass fraction Y, and the diffusion coefficients for the solar rotating models A_S (dotted lines) and A'$_S$ (solid lines) at 4.6 Gyr. The hatched areas indicate the convective envelope.

(A color version of this figure is available in the online journal.)

chemical species below the convective envelope in the models with slow rotation. This shows up in the helium mass fraction profile presented in quadrant III of Figure 5. There, the step in the helium profile at the base of the convective zone reveals the gravitational settling of helium in this region, and this, regardless of the existence of meridional flows and shear. If the young Sun was a slow rotator, the chemical stratification probed by helioseismic data in the region below the convective envelope would be the same as if the Sun had not rotated (provided that no other dynamical process than rotation is included).

Of course, one cannot ensure that the diffusivity coefficients are properly estimated, so it is interesting to see the impact of

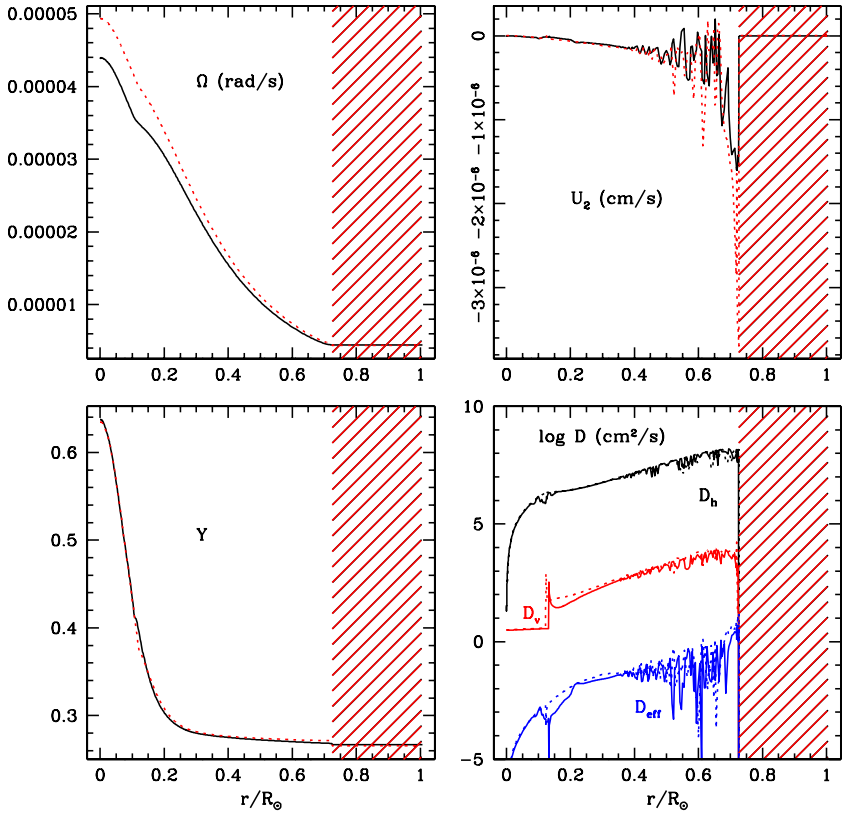

Figure 6. Profiles of the angular velocity Ω, the meridional circulation velocity U_2, the helium mass fraction Y, and the diffusion coefficients for the solar rotating models B_S (solid lines) and C_S (dotted lines) at 4.6 Gyr. The hatched areas indicate the convective envelope.

(A color version of this figure is available in the online journal.)

a different prescription for them. Using the STAREVOL code, we compute model A'$_S$ using the prescription of Zahn (1992) for D_h:

$$D_h = r[2V_2 - \alpha U_2]. \quad (11)$$

Figure 5 shows the profiles of the angular velocity Ω, the meridional circulation velocity U_2, the helium mass fraction Y, and the diffusion coefficients D_h, D_v, and $D_{\rm eff}$ for models A_S and A'$_S$. As expected, the horizontal turbulent diffusion coefficient D_h is 3 orders of magnitudes smaller when using Zahn's (1992) prescription (see also Mathis et al. 2004). This translates into an increase by the same amount of the effective diffusivity $D_{\rm eff}$. However, $D_{\rm eff}$ remains smaller than D_v and $\nu_{\rm mic}$ in model A'$_S$, so that the helium and angular velocity profiles remain unchanged compared to model A_S. From this comparison, we may conclude that in the case of a Sun that has always been rotating slowly, the choice of the prescription for the horizontal component of the shear-induced turbulent diffusivity does not affect significantly the structure, rotation and initial chemical stratification.

4.2. The Sun as a Mild Rotator on the ZAMS

We have also computed two models with a higher initial angular momentum, corresponding to a surface velocity of about 20 km s^{-1} and 50 km s^{-1} at the arrival on the ZAMS. These models undergo a strong angular momentum extraction on the early main sequence to reach a surface velocity of about 2 km s^{-1} at the age of the present Sun. This phenomenon associated to the idea of a magnetic braking due to the decoupling from the disk environment is modeled using the Kawaler formula as detailed in the previous section.

Figure 6 compares the results of the two models B_S and C_S at 4.6 Gyr. The diffusion coefficients D_v and $D_{\rm eff}$ entering the diffusion equation for the chemical species are similar in models B_S and C_S, so they lead to the same profile for the helium mass fraction. The angular velocity is slightly larger in the central regions in model C_S. This model is submitted to a more efficient braking in order to reach a surface velocity of about 2–2.2 km s^{-1} at the age of the Sun. In fact, when magnetic braking is initiated, the meridional circulation velocity U_2 is five times smaller in model C_S than that found in model B_S in absolute value, but it is positive (negative in model B_S) generating an efficient *inward* transport of angular momentum and leading to a faster and larger increase of the central velocity than in model B_S. The behavior found for model C_S is in all points similar to that reported by Eggenberger et al. (2005), and also resembles that described by Meynet & Maeder (2000) for more massive and fast rotating stars. The evolution further on the main sequence is similar for models B_S and C_S, with U_2 rapidly becoming negative in the later (see figure top right of Figure 6). The profiles displayed in Figure 6 show no significant difference for the diffusivities, meridional circulation, and helium profile at 4.6 Gyr, so that in the following we will focus on models B_S and model B_C.

The meridional velocity profiles at 4.6 Gyr for the B models are shown on the right panel of Figure 3. The velocity of the meridional currents is 3 orders of magnitude larger compared to models A_S and A_C previously described. At the ZAMS, the meridional circulation is maximal below the convective envelope as a result of the strong magnetic torque applied at the surface. U_2 is then 2 orders of magnitude larger than it will be later on the main sequence, when the efficient spin down of the surface layers is accompanied by a global weakening of the

meridional circulation. The form of the meridional circulation velocity profile U_2 is maintained over the main sequence evolution, and mainly consists in one counterclockwise cell peaking below the convective envelope and extracting angular momentum from the central regions, this time more efficiently than in the slowly rotating solar models. Similar to what was obtained by Decressin et al. (2009) for their 1.5 $M_\odot$ model, the meridional circulation is mainly driven by the local losses of angular momentum due to the magnetic braking. Meridional circulation and shear turbulence do not ensure an efficient transport of angular momentum. One notes that $U_{2,\max}$ is larger in model B_S by 25% compared to model B_C.

The gradient of angular velocity is much larger in these models compared to models A_C and A_S, and Ω increases by more than 1 order of magnitude from the surface to the solar core. We will discuss in more detail the implications of such a steep profile when confronted with helioseismic data. The match between the two codes shown in Figure 7 is not as good as that found for slowly rotating models. This is due to the difference in the numerical treatment used in both codes and the way the braking is introduced. The rotation profile is even steeper for models computed with CESAM, in which braking occurs very efficiently on the ZAMS so that the Ω-profile does not evolve at all in the last 3.6 Gyr. In model B_S, angular momentum is extracted from the central parts as the star evolves and both the central and surface values of the angular velocity decrease with increasing time so that the gradient is less steep at 4.6 Gyr than it is at 1 Gyr.

Diffusion coefficients are displayed in the right panel of Figure 4 at 4.6 Gyr. They have similar shapes and amplitude, which implies that the chemical stratification should also be similar in models B_S and B_C. Although U_2 is larger by 3 orders of magnitude compared to A models, the horizontal component of the turbulent diffusivity is also much larger leading to $D_{\rm eff}$ that is again smaller than 1 cm s^{-1}, which remains much smaller than both the local molecular diffusivity and the microscopic diffusivity. Meridional circulation is thus not contributing significantly to the transport of chemical species. On the other hand, in these mild rotating models, the Reynolds number associated with the sheared flow is larger than the critical Reynolds number Re_c, and the flow eventually becomes turbulent. The vertical turbulent diffusivity reaches values of the order of 100–1000 cm s^{-2} below the convective envelope, which is at least 10 times larger than the microscopic diffusivity in this region. As a consequence, the abundance profiles are flattened in both models B_S and B_C (see, e.g., see solid line in quadrant III of Figure 6 for model B_S), and thus differ significantly from those derived for SSMs. If the young Sun was a fast rotator and experienced magnetic braking during the early main sequence without any inhibition of the action of the shear-induced turbulent mixing, the chemical stratification of the present Sun below the convective zone might bear the signature of this past rotational history.

5. CONFRONTATION BETWEEN THEORETICAL AND OBSERVATIONAL PROFILES

5.1. The Solar Observed Rotation Profile

After more than 10 years of observations with GOLF and MDI instruments located onboard *SoHO*, and with the facilities of the GONG ground-based network, we have derived very important constraints on the radiative zone rotation profile. The determination of the splittings of a large number of acoustic

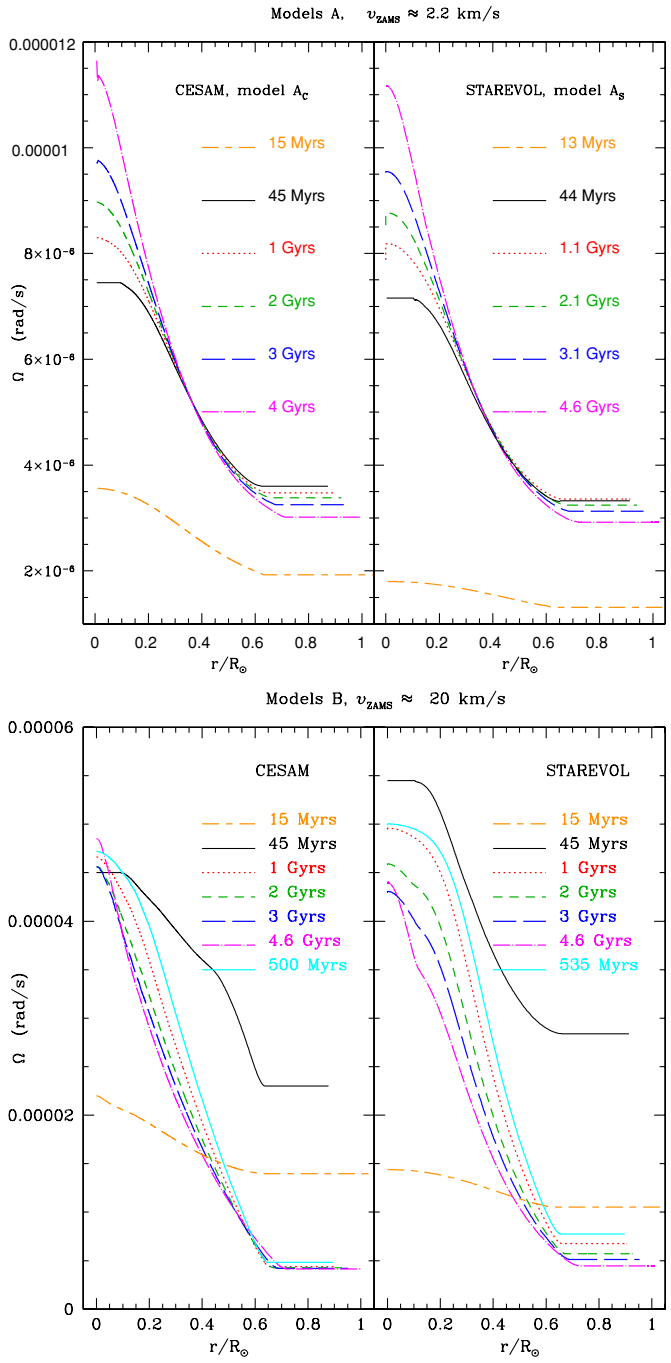

Figure 7. Evolution of the angular velocity profiles at six different ages as indicated on the plots, for models A_C and A_S (left panels) and B_C and B_S (right panels). The age of 45 Myr corresponds to the arrival on the main sequence.

(A color version of this figure is available in the online journal.)

modes has definitely established that the rotation profile in the part of the radiative zone which is not influenced by the nuclear reaction rates, e.g., the region between 0.25 and 0.68 $R_\odot$, is really flat with invisible latitudinal differential variation (Couvidat et al. 2003b; Eff-Darwich et al. 2008), in great contrast with the latitudinal differential profile of the convective zone. In the central region, below 0.25 $R_\odot$, only gravity modes may inform the rotation profile. Some individual candidate modes at high frequency have been observed by the GOLF instrument (Turck-Chièze et al. 2004b; Mathur et al. 2007; García et al. 2008), and two solutions have been extracted from these first data depending on the interpretation of the pattern

Table 5
Characteristics of the Models Computed with CESAM for an Initial Rotation of 20 km s^{-1}

Age (Gyr)	R ($R_\odot$)	L ($L_\odot$)	E_G (%)	E_{pp} (%)	$E_{\rm CNO}$ (%)	T_c	ρ_c	$\upsilon_{\rm c,eq}$ (km s^{-1})	$\upsilon_{\rm s}$ (km s^{-1})
0	17. 36	72.4	100	0	0	4.8×10^5	2.05×10^{-3}	0.47	0.47
0.00001	10.62	32.5	100	0	0	7.58×10^5	8.26×10^{-3}		0.74
0.0001	4.95	8.6	100	0	0	1.58×10^6	7.55×10^{-2}		1.51
0.001	2.28	1.92	100	0	0	3.38×10^6	0.73		3.18
0.005	1.36	0. 63	100	0	0	5.32×10^6	4.1		5.51
0.011	1.12	0. 46	100	0	0	6.62×10^6	12.15		7.99
0.026	1.024	0.897	69	31	0	11.9×10^6	75.53		16.78
0.039	0.88	0.71	0	93	7	13.58×10^6	79.18		20.25
0.045	0.87	0.69	0	93	7	13.56×10^6	78.68	26.7	19.6
0.147	0.88	0.72	0	98	2	13.5×10^6	82.6	30.8	5.
1	0.9	0.76	0	100	0	13.8×10^6	91.		2.19
2	0.921	0.82	0	100	0	14.2×10^6	102.4	38.8	2.08
3	0.945	0.88	0	100	0	14.7×10^6	116.4	37.3	2.086
4.6	0.992	1.000	0	99	1	15.61×10^6	146.6	39.	2.09

attributed to an $\ell = 2$, $n = 2$ mode: a slightly reduced rotation rate or an increase by about a factor 3 in the central region (Mathur et al. 2008). Nevertheless, only the solution of a rapid rotating core is compatible with the other kind of detection using the asymptotic behavior at low frequency which is detected with a very high probability (García et al. 2007, 2008). It could presume a rather complex solar core rotation larger than the rest of the radiative zone, with a different axis, and maybe with some manifestation of the radiative zone magnetic field. The other solution cannot be totally excluded but is not the most probable. Again, the core profile needs to be confirmed with extensive data from *SoHO* and with an improved instrument like the GOLF-NG concept (Turck-Chièze et al. 2006, 2008) which will measure velocity displacements at eight heights in the solar atmosphere. Considering that the complete solar rotation profile might be accessible to observation, it is important to predict it properly down to the central region.

5.2. The Theoretical Solar Rotation Profile

This paper is a new step toward a detailed understanding of how the different dynamical processes can influence the present rotation of the Sun. In this study we have followed three different cases because we can only have some indirect information on the solar internal rotation profile at the end of its contraction phase. We have already seen in the previous section that the initial angular momentum content and the rotation history, in particular the fact of undergoing magnetic braking on the ZAMS, shape the angular velocity profile, determining the absolute value as well as the gradient. In this section, we wish to focus on the evolution of the angular velocity profile. We present hereafter a detailed analysis of the construction of the predicted internal profile at the age of the Sun and confront these predictions with helioseismology.

Compared to previous studies by Eggenberger et al. (2005) and Talon & Charbonnel (2005) where rotation was only included from the ZAMS, with an initial flat profile, we have decided to follow rotation from the PMS when the star is actually completely convective. We also assume solid-body rotation as the initial state, but by the time the models reach the ZAMS, the convective region has retreated to the surface and the Ω-profile is not flat anymore.

Tables 4 and 5 list the evolution of the radius, the luminosity, the central and the superficial velocity for models A_C and B_C, and some other indicators of the contraction phase and of the involved nuclear reactions. The evolution of the angular velocity profile for these models is also presented in the left panels of Figure 7.

For model A_C, where the initial rotation rate is of about 0.08 km s^{-1}, the contraction of the star during the PMS rapidly generates a radial gradient in the Ω-profile. The very slow meridional currents and the small amount of shear generated in such slowly rotating models are not very efficient to transport the angular momentum. The differential rotation established during the early evolution by the contraction of the inner regions is maintained and slightly amplified during the main sequence by the advection term. The predicted overall contrast between core and surface velocities is of about a factor of 4, which is comparable to that obtained by Eggenberger et al. (2005) in their slowly rotating model.

Models B and C are similar to those presented in the three main previous studies of the effect of rotation on the solar evolution by Chaboyer et al. (1995), Eggenberger et al. (2005), and Charbonnel & Talon (2005). The evolution of the angular velocity profile is in agreement with that obtained in the later study, where STAREVOL models were also used. Comparing the evolution displayed in Figure 7 with that of Figures 1 and 2 of Charbonnel & Talon (2005) and Eggenberger et al. (2005), respectively, one can measure the impact of the numerical approach. In all these cases, if the general forms and amplitudes of the angular velocity profile at the age of the Sun show encouraging similarities (see also Figure 8), the in between evolution can be quite different. Models B_S and B_C undergo a very strong braking at the arrival on the ZAMS leading to a quick spin down of the convective envelope and a contrast between the surface and central angular velocities of about a factor 15 for model B_C already at 1 Gyr, and of about 7 in model B_S at the same age. In the later model, the contrast increases during the main sequence to reach a factor of 10 between the core and the surface at 4.6 Gyr. In both models, the Ω-gradient steepens in the bulk of the radiative zone as the star evolves. The profiles are flatter in model B_S, yet not as flat as those presented in Figure 2 of Eggenberger et al. (2005).

A detailed analysis of the relative importance of meridional circulation versus shear-turbulence in our models A_S, B_S, and C_S using the tools presented in Decressin et al. (2009), demonstrates that the behavior of these solar models is in all points similar to that obtained for the 1.5 $M_\odot$ model shown in that paper. The angular momentum transport is ensured by meridional currents. In the case of models B and C, these currents, although slow, are primarily generated by the action of the applied torques

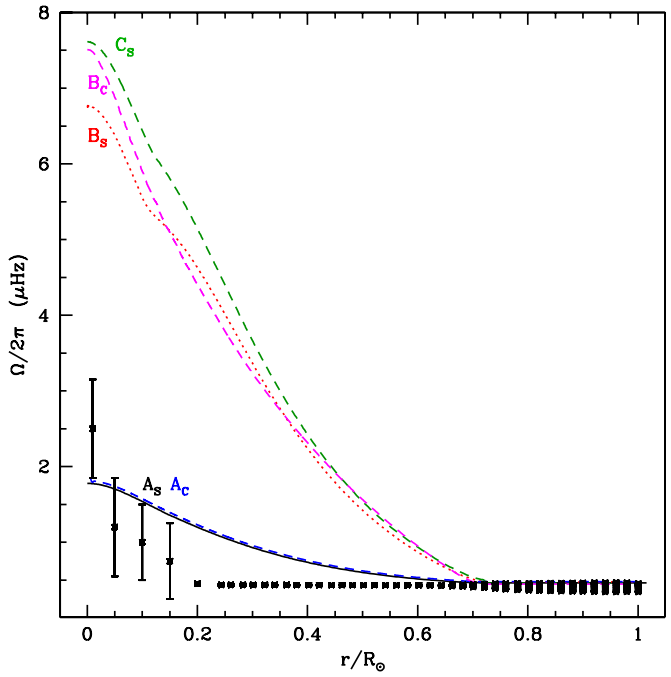

Figure 8. Comparison between the solar internal profile predicted by the different models and that deduced from helioseismology. For models B_S and C_S, the actually plotted value is $\Omega/2\pi$-0.2325 rather than $\Omega/2\pi$ in order for the surface value they reach to match that reached by model B_C. The data points down to $r/R_\odot = 0.2$ are deduced from the acoustic mode splittings determined by the observations of GOLF, MDI, and GONG instruments (from Eff-Darwich et al. 2008). The data points in the core correspond to the supposed core rotation extracted from the potentially observed gravity modes. These values have still large error bars and need to be confirmed (inspired by Turck-Chièze et al. 2004b; García et al. 2007; Mathur et al. 2008).

(A color version of this figure is available in the online journal.)

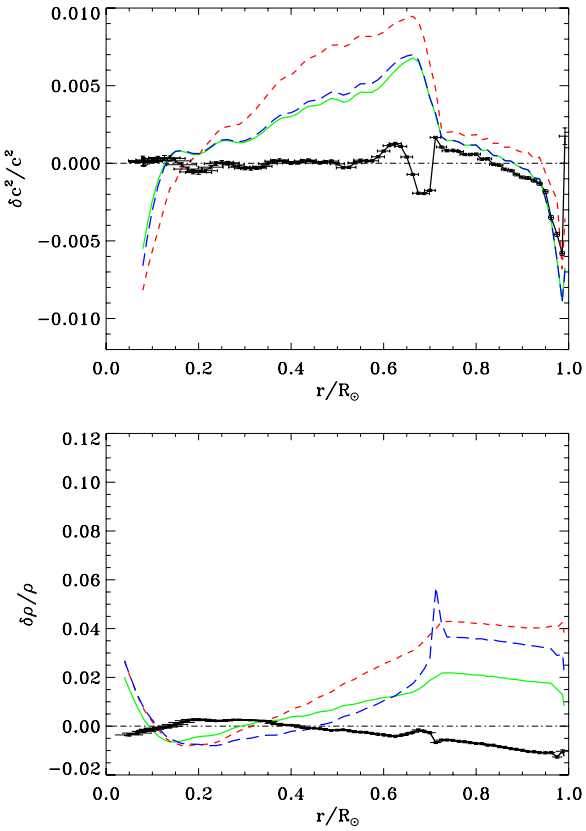

Figure 9. Radial squared sound speed and density differences between observations and models computed with the CESAM code. Seismic model (Turck-Chièze et al. 2001b, 2004a) is in black with error bars coming from the seismic data. The present models (standard GN composition) without rotation, with low rotation (model A), or moderate rotation, of 20 km s^{-1} initial model with a magnetic break of the surface at the arrival on the main sequence (model B) are, respectively, in green (dotted dashed line), blue (large dashed line), and red (small dashed line).

(A color version of this figure is available in the online journal.)

resulting from the action of magnetic braking. In the case of the slow model A, no torque is applied and the angular momentum flux is smaller yet also dominated by the meridional circulation. The flux of angular momentum due to shear turbulence is more than 5 orders of magnitude smaller than that attributed to the meridional circulation in all three cases.

5.3. Discussion

These detailed calculations are self-consistent and rely on the use of a set of parameters that have been extensively tested throughout the H-R diagram. They consider initial rotation generally smaller than used in the previous literature (Chaboyer et al. 1995; Krishnamurthi et al. 1997) and show slower differential rotations in the core than found in previous works (Pinsonneault et al. 1989) or the most recent of Charbonnel & Talon (2005). Figure 8 shows a first comparison between the different profiles and the presumed observed rotation profile. It is clear that the models with an initial reasonable rotation velocity + magnetic braking are not supported by the observations. As indicated by García et al. (2007), the helioseismic data reject an increase by a factor 10 for the core rotation. On the contrary, the slow initial rotation leads to a profile for the present Sun for which the contrast between the core and the surface angular velocity is very similar to the presumed observed one. The contrast is similar but of course none of the different models investigated here create a flat rotation between 0.25 and 0.7 solar radius. Within the framework of the present study, models A_S and A_C corresponding to an extremely slow rotating young Sun are more compatible with the central observations. However, this cannot be taken at face value because this model seems rather unrealistic because it did not contain any magnetic braking (see Figure 2 of Bouvier 2009). So, one can imagine a slightly greater initial rotation, typically 5 or 10 km s^{-1} at the ZAMS, with a central rotation value slightly eroded by some other process. The discrepancy between helioseismology and the profiles presented here calls for the inclusion of additional dynamical processes that efficiently extract angular momentum from the radiative interior. This result confirms the most recent works. Probably the radiative magnetic field (Eggenberger et al. 2005; Yang & Bi 2006; Denissenkov & Pinsonneault 2007) or the internal gravity waves (Charbonnel & Talon 2005), or both, could flatten the profile, but their role could be smaller than thought previously.

5.4. The Sound Speed Profile, Composition, and Neutrino Predictions

Figure 9 compares the squared sound speed profile difference between seismic observations and the models computed with CESAM. The used acoustic modes are given in Couvidat et al. (2003a). We present the three models (standard, low rotation, and moderate rotation) computed with the version of CESAM used in the present study. These models slightly differ from the standard models already published due to the large reduction of the (^{14}N, p) reaction rate mentioned in Section 2. The CNO combustion is rather small, but this strong decrease, previously

Table 6
Comparison of the Different Models Computed With the CESAM and STAREVOL Codes

Model	CESAM Seismic	CESAM SSM	CESAM Slow (A)	CESAM Moder. (B)	STAREVOL Slow (A)	STAREVOL Moder. (B)	STAREVOL Fast (C)
X_i	0.7064	0.7075	0. 7078	0.7117	0.7015	0.7015	0.7015
Y_i	0.2722	0.2729	0.2727	0.2690	0.280	0.280	0.280
X_c	0.3371	0.361	0.364	0.3522	0.3397	0.3422	0.3456
Y_c	0.6428	0.618	0.615	0.6301	0.609	0.6376	0.6341
T_c	15.71	15.64	15.63	15.54	15.67	15.63	15.55
ρ_c	153.7	147.8	147.1	146.	155.3	154.4	153.1
Y_s	0.251	0.245	0.242	0.253	0.248	0.267	0.265
α	2.04	1.77	1.77	1.725	1.7378	1.7378	1.7378
$r_{\rm BZC}$	0.7113	0.714	0.715	0.7241	0.719	0.7228	0.7235
$(Z/X)_s$	0.0245	0.0245	0.0245	0.0245	0.0230	0.0250	0.0247

Notes. X_i and Y_i are, respectively, the initial hydrogen and helium mass fractions. X_c, Y_c, T_c, and ρ_c are, respectively, the present central hydrogen, helium, temperature, and density. Y_s is the present superficial helium mass fraction, α is the mixing length parameter, r_{BZC} is the position of the base of the convective zone, $(Z/X)_s$ is the mass fraction of the heavy element in considering the GN composition. The CESAM models are all calibrated.
[a] The indices i and s are for initial and surface, the central temperature T_C is in million degrees, boron flux in 10^6 cm^{-2} s^{-1}.

studied in Turck-Chièze et al. (2001a), leads to a negative sound speed difference in the core partly compensated by a small increase in the rest of the radiative zone. These two differences increase the difference with observations. But what we would like to emphasize in this figure is the intercomparison between models with and without rotation.

Even if these models must be more representative of the real Sun, the sound speed profile obtained for the two calibrated CESAM rotating models A and B is in less agreement with the observed profile than the standard model. In fact, the rotation-induced mixing has reduced the effect of the microscopic diffusion (see also Section 4) partly inhibited by the macroscopic motions. As discussed earlier, such an effect is practically not visible in models A, where microscopic diffusivity remains larger than both the vertical turbulent and the effective diffusivity, but it is clearly visible in models B and C rotating faster on the ZAMS.

As a natural consequence, Table 6 shows also that the central temperature is slightly reduced in rotating models in comparison with the SSM. For the CESAM models calibrated in radius and luminosity at 10^{-4} level, the predictions for the neutrinos are always worse than those of the seismic model (see details in Table 1). Moreover, in CESAM models where we have kept superficial Z/X constant, one may notice that the surface helium content also increases with the initial rotation due to turbulent flow just below the convective zone, as previously mentioned in Section 4 for the STAREVOL results but by a smaller amount (comparison of the two codes in Table 6). This will contribute to reconciling the observed helium content to the predicted one when using the most recent composition of Asplund et al. (2009), if the initial rotation is sufficient to allow turbulent flow at the base of the convective zone and in the tachocline.

6. CONCLUSION AND PERSPECTIVES

In this paper we have shown the following facts:

1. We have examined three initial rotation rates (models A, B, and C), choosing initial angular momentum contents corresponding to 2.5 km s^{-1}, 20 km s^{-1}, and 50 km s^{-1} at the ZAMS. The last two values have also been adopted in other studies of the rotating Sun and solar-type stars (Yang & Bi 2006; Eggenberger et al. 2005; Talon & Charbonnel 2005; Chaboyer et al. 1995). At 4.6 Gyr, the three cases show a radial gradient of rotation in the core. Its amplitude depends strongly on the initial rotation rate. If this one is small, the radial gradient is established during the contraction phase and is amplified during the subsequent evolution up to the present Sun. For models rotating faster, one notes much steeper gradients at the age of the Sun; the angular momentum losses associated with magnetic braking on the ZAMS are responsible for the rather small decrease on the ZAMS.
2. The transport of angular momentum in the solar radiative zone during the main sequence appears extremely small and the meridional circulation in the radiative zone is smaller by 10 orders of magnitude in comparison with the observed convective meridional circulation velocity at 99% $R_\odot$. This process is even slower than the microscopic diffusion (gravitational settling) that we use in the radiative zone. As a first consequence, such implementation in a stellar evolution code is delicate mainly because one needs to solve four coupled equations with derivation of quantities that practically do not vary. In order to settle our conclusions concerning the form and order of magnitude of the different quantities associated to the rotation-induced mixing, we have confronted models obtained with two different codes, CESAM and STAREVOL, using distinct numerical approaches and the old composition of Grevesse and Noels. We have shown, for models A and B, that they lead to rather similar results and the same kind of profile for the present Sun, thus validating the results and numerical approaches. Such a very large difference between the meridional velocity in the radiative zone (10^{-7}–10^{-6} cm s^{-1}) and in the convective zone (m s^{-1}) would naturally produce some turbulent hydrodynamical layer generally called tachocline and this is an interesting result of the present calculation.
3. Although the combined effect of meridional circulation and shear-induced turbulence associated to rotation is small, this study allows us to present radial rotation profiles that can be directly compared to the seismically observed one. This study sustains the idea that the Sun was not at the beginning a rapid rotator. The angular velocity profile we get for the A models is not far from the presumed solar one in the core. Of course this model should not be considered at face value since it does not take into account any magnetic braking

generally observed in young clusters, but it can be useful to estimate the interplay between processes. The second model (moderate rotation) is more realistic but shows a greater steep gradient in disagreement with the published detection of gravity modes. So, one can imagine that the Sun has been in an intermediate case arriving at 5–10 km s^{-1} at ZAMS and that its rotation profile would have being eroded by some other process.

4. Let us stress, however, that other dynamical processes known to generate efficient transport of angular momentum such as magnetic fields and internal gravity waves were not yet included in our models. The inclusion of these processes is in the scope of a further study, and is expected to significantly affect the choice of the preferred model. For instance, internal fossil magnetic field certainly produces a very small effect on the solar structure (Duez et al. 2010a) but may lead to efficient transport of angular momentum that would help flattening the angular velocity profile in the radiative zone. But first, we would like to study the activity of the very young Sun. Previous works show how magnetic field can modify the rotation profile (Eggenberger et al. 2005; Denissenkov & Pinsonneault 2007) but the action could be improved by the introduction of a more sophisticated field topology which preserves the stability of such a field (Duez & Mathis 2010). The understanding of the magnetic field during the contraction phase probably has a crucial impact on the radial rotation gradient and deserves a premature estimate of lithium and beryllium destruction at this stage.
5. Other processes may modify the present conclusions. For example, in the present treatment we neglect the fundamental role of the tachocline which must be established at least since the arrival on the main sequence. The hydrodynamical (or magnetohydrodynamical) nature of such a region may alter the angular momentum and/or chemicals transport due to the internal rotation, but we have already noticed that a crude treatment of this region might slightly amplify the present tendency on the chemicals gradient and structure effect (Brun et al. 1999). In the present study, we note that if the initial rotation is accompanied by an efficient magnetic braking, it generates some turbulent flow at the base of the convective zone which smoothes the helium profile and increases its abundance at the surface.
6. We note that the impact of the rotation on the solar structure is rather small. As the transport of angular momentum and chemicals goes from the radiative zone to the convective zone, it implies a slight reduction of the central temperature and of the helium content in the radiative zone. Consequently, it increases slightly the present discrepancy between the model and the observed sound speed. In fact, one cannot exclude other momentum transport which may come from the convective zone and play the inverse role (Garaud & Garaud 2008; Gough 2010). All these other processes must be included in stellar evolution codes before getting a proper DSM. We see in this study that the description of the dynamics of the PMS phase (especially the related magnetic field evolution) will be a crucial issue too. In the comparison between CESAM and STAREVOL, we have noticed some nonnegligible difference during the contraction phase for models with a moderate (the same for high) initial rotation rate; this phase illustrates the sensitivity of the rotation gradient to the numerical details and to the magnetic braking. Moreover, we show in this study that independently of the initial rate, the central rotation value does not change by more than 50% during the main sequence. So the final comparison of the DSM to the observations will partly depend on the way we shall treat the contraction phase, the inner corresponding magnetic field evolution and the magnetic braking phase. The same conclusion was already reached discussing the problem of lithium in young stars and in the Sun (Brun et al. 1999; Piau & Turck-Chièze 2002).
7. The sound speed profile is practically unchanged when the slow initial rotation is assumed. So, even if this model is probably more representative of the dynamics of the solar interior than the standard model, it is still an incomplete model and its predictive character remains limited. For this reason, and considering the consequent discrepancy on the sound speed predicted by the present standard model and the observed one, which will be amplified by the recent CNO composition, we continue to recommend the seismic model for any global predictions (gravity modes or neutrinos). We have shown in this paper that the predictions of the seismic model are in very good agreement with all the neutrino detections including BOREXINO.

We thank Pierre Morel for his dedicated effort to introduce the dynamical processes in CESAM code, Stephane Mathis and Jean Paul Zahn for very interesting discussions, and the anonymous referee for helping us to improve the paper.

REFERENCES

Adelberger, E., et al. 1998, Rev. Mod. Phys., 70, 1265
Ahmed, S. N., & The SNO Collaboration 2004, Phys. Rev. Lett., 92, 181301
Alexander, D. R., & Ferguson, J. W. 1994, ApJ, 437, 879
Arpesella, C., & The Borexino Collaboration 2008, Phys. Rev. Lett., 101, 091302
Asplund, M., Grevesse, N., Sauval, A. J., Allende Prieto, C., & Kiselman, D. 2004, A&A, 417, 751
Asplund, M., Grevesse, N., & Scott, P. 2009, ARA&A, 47, 481
Bahcall, J. N., & Pena-Garay, C. 2004, New J. Phys., 6, 63
Bahcall, J. N., & Pinsonneault, M. H. 1995, Rev. Mod. Phys., 67, 781
Bahcall, J. N., Serenelli, A. M., & Basu, S. 2005, ApJ, 621, L85
Bailey, J., et al. 2007, Phys. Rev. Lett., 99, 5002
Basu, S., & Antia, H. M. 1995, MNRAS, 276, 1402
Basu, S., & Antia, H. M. 2008, Phys. Rep., 457, 217
Basu, S., et al. 2007, ApJ, 655, 660
Bertello, L., Varadi, F., Ulrich, R. K., Henney, C. J., Kosovichev, A. G., García, R. A., & Turck-Chièze, S. 2000, ApJ, 537, L143
Bouvier, J. 1994, in ASP Conf. Ser. 64, Cool Stars, Stellar Systems, and the Sun; Eighth Cambridge Workshop, ed. J.-P. Caillault (San Francisco, CA: ASP), 151
Bouvier, J. 2009, in Stellar Magnetism, ed. C. Neiner & J.-P. Zahn (EAS Publication Series; Noordwijk: ESA), 199
Bouvier, J., Forestini, M., & Allain, S. 1997, A&A, 326, 1023
Brun, A. S., Turck-Chièze, S., & Morel, P. 1998, ApJ, 506, 913
Brun, A. S., Turck-Chièze, S., & Zahn, J. P. 1999, ApJ, 525, 1032
Busse, F. H. 1982, ApJ, 259, 759
Caffau, E., Ludwig, H.-G., Steffen, M., Ayres, T. R., Bonifacio, P., Cayrel, R., Freytag, B., & Plez, B. 2008, A&A, 488, 1031
Caffau, E., et al. 2009, A&A, 498, 877
Chaboyer, B., Demarque, P., & Pinsonneault, M. H. 1995, ApJ, 441, 865
Chaboyer, B., & Zahn, J.-P. 1992, A&A, 253, 173
Charbonnel, C., & Talon, S. 2005, Science, 309, 2189
Christensen-Dalsgaard, J., Proffitt, C. R., & Thompson, M. J. 1993, ApJ, 403, L75
Couvidat, S., Garcia, R. A., Turck-Chièze, S., Corbard, T., Henney, C. J., & Jimenez-Reyes, S. 2003b, ApJ, 597, L77
Couvidat, S., Turck-Chièze, S., & Kosovichev, A. G. 2003a, ApJ, 599, 1434
Cox, A. N., Guzik, J. A., & Kidman, R. B. 1989, ApJ, 342, 1187
Decressin, T., & Charbonnel, C. 2005, From Lithium to Uranium: Elemental Tracers of Early Cosmic Evolution (Cambridge: Cambridge Univ. Press), 395

Decressin, T., Mathis, S., Palacios, A., Siess, L., Talon, S., Charbonnel, C., & Zahn, J. 2009, A&A, 495, 271
Denissenkov, P. A., & Pinsonneault, M. 2007, ApJ, 655, 1157
Domiciano de Souza, A. 2008, in The Rotation of Sun and Stars (Lect. Notes Phys. 765), ed. J. P. Rozelot & C. Neiner (Berlin: Springer), 171
Domiciano de Souza, A., Kervella, P., Jankov, S., Abe, L., Vakili, F., di Folco, E., & Paresce, F. 2003, A&A, 407, L47
Duez, V., & Mathis, S. 2010, A&A, in press
Duez, V., Mathis, S., & Turck-Chièze, S. 2010a, MNRAS, 402, 271
Duez, V., Turck-Chièze, S., & Mathis, S. 2010b, ApJL, submitted
Dzitko, H., Turck-Chieze, S., Delbourgo-Salvador, P., & Lagrange, C. 1995, ApJ, 447, 428
Eff-Darwich, A., Korzennik, S. G., Jiménez-Reyes, S. J., & García, R. A. 2008, ApJ, 679, 1636
Eggenberger, P., Maeder, A., & Meynet, G. 2005, A&A, 440, L9
Eggenberger, P., Meynet, G., Maeder, A., Hirschi, R., Charbonnel, C., Talon, S., & Ekström, S. 2008, Ap&SS, 316, 43
Endal, A. S., & Sofia, S. 1981, ApJ, 243, 625
Formicola, A., et al. 2004, Phys. Lett. B, 591, 61
Fröhlich, C. 2006, Space Sci. Rev., 125, 53
Gabriel, A. H., et al. 1995, Sol. Phys., 162, 61
Garaud, P., & Garaud, J-D. 2008, MNRAS, 391, 1239
García, R. A., Turck-Chièze, S., Jiménez-Reyes, S. J., Ballot, J., Pallé, P. L., Eff-Darwich, A., Mathur, S., & Provost, J. 2007, Science, 316, 1591
García, R. A., et al. 2001, Sol. Phys., 200, 361
García, R. A., et al. 2008, Astron. Nachr., 329, 476
Gough, D. 2010, in Astrophysics and Space Science Proc., Magnetic Coupling between the Interior and the Atmosphere of the Sun, ed. S. S. Hasan & R. J. Rutten (Berlin: Springer), 67
Grevesse, N., & Noels, A. 1993, Origin and Evolution of the Elements (Cambridge: Cambridge Univ. Press), 14
Guzik, J. A., & Mussak, K. 2010, ApJ, 713, 1108
Guzik, J. A., Watson, L. S., & Cox, A. N. 2005, ApJ, 627, 1049
Heger, A., Langer, N., & Woosley, S. E. 2000, ApJ, 528, 368
Henyey, L. G., Forbes, J. E., & Gould, N. L. 1964, ApJ, 139, 306
Hill, H., Froehlich, C., Gabriel, M., & Kotov, V. A. 1991, Solar Interior and Atmosphere (A92-36201 14-92; Tucson, AZ, Univ. Arizona Press), 562
Holweger, H. 2001, in AIP Conf. Proc. 598, Solar and Galactic Composition, ed. R. F. Wimmer-Schweingruber (Melville, NY: AIP), 23
Igamov, S. B., & Yarmukhamedov, R. 2008, Phys. At. Nuclei, 71, 1740
Iglesias, C. A., & Rogers, F. J. 1996, ApJ, 464, 943
Iglesias, C. A., & Rose, S. J. 1996, ApJ, 466, L115
Itoh, N., Hayashi, H., Nishikawa, A., & Kohyama, Y. 1996, ApJS, 102, 411
Junghans, A. R., Mohrmann, E. C., & Snover, K. A. 2005, Nucl. Phys., 138, 112
Kawaler, S. D. 1988, ApJ, 333, 236
Kervella, P., & Domiciano de Souza, A. 2006, A&A, 453, 1059
Kopp, G., Lawrence, G., & Rottman, G. 2005, Sol. Phys., 230, 129
Kosovichev, A. G., et al. 1997, Sol. Phys., 170, 43
Kraft, R. P. 1965, ApJ, 142, 681
Krishnamurthi, A., et al. 1997, ApJ, 480, 303
Langer, N. 1998, A&A, 329, 551
Lin, C.-H., Antia, H. M., & Basu, S. 2007, ApJ, 668, 357
Loisel, G., et al. 2009, High Energy Density Phys., 5, 173
Lydon, & Sofia, S. 1995, ApJS, 101, 603
Maeder, A., & Meynet, G. 2000, ARA&A, 38, 143, 1063
Maeder, A., & Meynet, G. 2004, A&A, 422, 225
Maeder, A., & Zahn, J.-P. 1998, A&A, 334, 1000
Marques, J. 2010, A&A, submitted
Mathis, S., Palacios, A., & Zahn, J.-P. 2004, A&A, 425, 243 (erratum 462 [2007])
Mathis, S., Talon, S., Pantillon, F.-P., & Zahn, J.-P. 2008, Sol. Phys., 251, 101
Mathis, S., & Zahn, J.-P. 2004, A&A, 425, 229
Mathur, S., Eff-Darwich, A., Garcia, R. A., Korzennik, S. G., & Turck-Chieze, S. 2008, A&A, 484, 517
Mathur, S., Turck-Chièze, S., Couvidat, S., & García, R. A. 2007, ApJ, 668, 594
McAlister, H. A., et al. 2005, ApJ, 628, 439
Meynet, G., & Maeder, A. 2000, A&A, 361, 101
Michaud, G., et al. 2004, ApJ, 606, 452
Montmerle, T., & Michaud, G. 1976, ApJS, 31, 489
Morel, P. 1997, A&AS, 124, 597
Palacios, A., Charbonnel., C., Talon, S., & Siess, L. 2006, A&A, 453, 261
Palacios, A., Talon, S., Charbonnel, C., & Forestini, M. 2003, A&A, 399, 603
Paquette, C., Pelletier, C., Fontaine, G., & Michaud, G. 1986, ApJS, 61, 177
Piau, L., & Turck-Chièze, S. 2002, ApJ, 566, 419
Pinsonneault, M. H., Kawaler, S. D., Sofia, S., & Demarque, P. 1989, ApJ, 338, 424
Richard, D., & Zahn, J. P. 1999, A&A, 347, 734
Rozelot, J. P. 2009, in The Rotation of Sun and Stars (Lect. Notes Phys. 765), ed. J.-P. Rozelot & C. Neiner (Berlin: Springer), 15
Scherrer, P. H., et al. 1995, Sol. Phys., 162, 129
Serenelli, A., et al. 2009, ApJ, 705, L123
Siess, L. 2006, A&A, 448, 717
Siess, L., Dufour, E., & Forestini, M. 2000, A&A, 358, 593
Sills, A., Pinsonneault, M. H., & Terndrup, D. M. 2000, ApJ, 534, 335
Skumanich, A. 1972, ApJ, 171, 565
Stauffer, J. R., Hatmann, L. W., Lee, W., & Latham, D. W. 1987, ApJ, 320L, 51
Talon, S., & Charbonnel, C. 1998, A&A, 335, 959
Talon, S., & Charbonnel, C. 2005, A&A, 440, 981
Talon, S., & Zahn, J.-P. 1997, A&A, 317, 749
Thompson, M. J., Christensen-Dalsgaard, J., Miesch, M. S., & Toomre, J. 2003, ARA&A, 41, 599
Thoul, A. A., Bahcall, J. N., & Loeb, A. 1994, ApJ, 421, 828
Thuillier, G. 2005, Mem. Soc. Astron. Ital., 76, 901
Turck-Chièze, S. 1998, Space Sci. Rev., 85, 125
Turck-Chieze, S. 2004, Nucl. Phys. B Suppl., 143, 35
Turck-Chièze, S., Cahen, S., Casse, M., & Doom, C. 1988, ApJ, 335, 415
Turck-Chièze, S., Couvidat, S., & Piau, L. 2005, in Element Stratification in Stars: 40 Years of Atomic Diffusion (EAS Pub. Ser. 17), ed. G. Alecian, O. Richard, & S. Vauclair (Les Ulis, France: EDP Sciences), 149
Turck-Chièze, S., Couvidat, S., Piau, L., Ferguson, J., Lambert, P., Ballot, J., García, R. A., & Nghiem, P. 2004a, Phys. Rev. Lett., 93, 211102
Turck-Chièze, S., Däppen, W., Fossat, E., Provost, J., Schatzman, E., & Vignaud, D. 1993, Phys. Rep., 230, 57
Turck-Chièze, S., & Lambert, P. 2007, Adv. Space. Res, 40, 907
Turck-Chièze, S., & Lopes, I. 1993, ApJ, 408, 347
Turck-Chièze, S., & Lefebvre, S. 2010, JASTP, in press
Turck-Chièze, S., Nghiem, P., Couvidat, S., & Turcotte, S. 2001a, Sol. Phys., 200, 323
Turck-Chièze, S., Piau, L., & Couvidat, S. 2010, ApJL, submitted
Turck-Chièze, S., & the GOLF-NG collaboration 2006, Adv. Space Res., 38, 1812
Turck-Chièze, S., & the GOLF-NG Collaboration 2008, J. Phys. Conf. Ser., 118, 012044
Turck-Chièze, S., et al. 1997, Sol. Phys., 175, 247
Turck-Chièze, S., et al. 2001b, ApJ, 555, L69
Turck-Chièze, S., et al. 2004b, ApJ, 604, 455
Turck-Chièze, S., et al. 2009, High Energy Density Phys., 5, 132
van Belle, G. T., et al. 2006, ApJ, 637, 494
Vorontsov, S. V., Baturin, V. A., & Pamiatnykh, A. A. 1991, Nature, 349, 49
Weber, E. J., & Davis, L., Jr. 1967, ApJ, 148, 217
Yang, W. M., & Bi, S. L. 2006, A&A, 449, 1161
Yang, W. M., & Bi, S. L. 2007, ApJ, 658, L67
Zahn, J.-P. 1992, A&A, 265, 115
Zahn, J.-P. 2009, in The Rotation of Sun and Stars (Lect. Notes Phys. 765), ed. J.-P. Rozelot & C. Neiner (Berlin: Springer), 1
Zahn, J.-P., Talon, S., & Matias, J. 1997, A&A, 322, 320